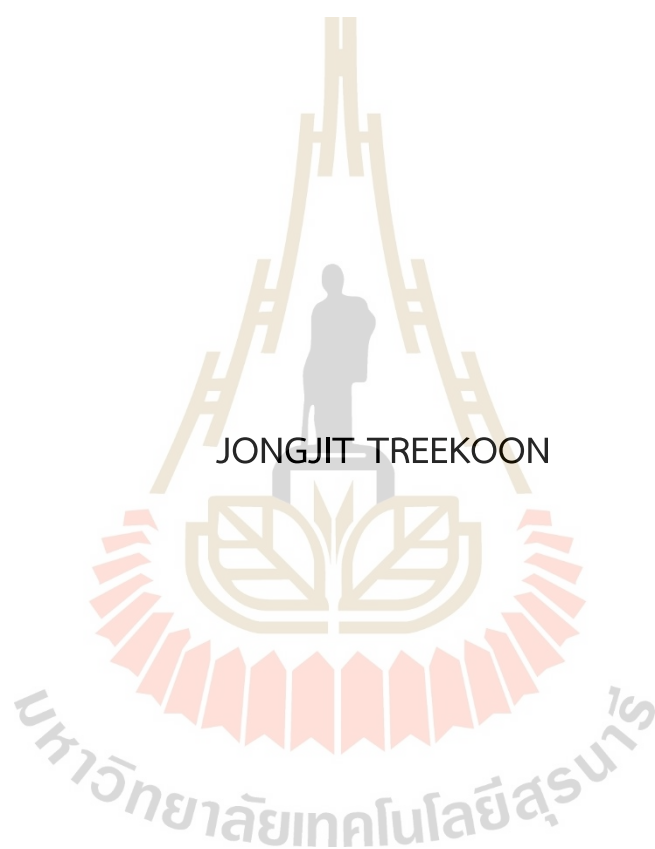


GLUCOSE CONJUGATED NEAR INFRARED DYES FOR
PHOTODYNAMIC THERAPY IN CANCER CELLS



A Thesis Submitted in Partial Fulfillment of the Requirements for the
Degree of Master of Science in Chemistry
Suranaree University of Technology
Academic Year 2021

กลุ่คอสเชื่อมต่อกับสารเรืองแสงช่วงใกล้อินฟราเรดสำหรับการรักษาโดยใช้
แสงเป็นตัวกระตุ้นในเซลล์มะเร็ง



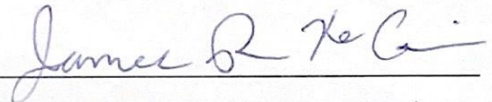
นางสาวจงจิต ตรีกุล

วิทยานิพนธ์นี้เป็นส่วนหนึ่งของการศึกษาตามหลักสูตรปริญญาวิทยาศาสตรมหาบัณฑิต
สาขาวิชาเคมี
มหาวิทยาลัยเทคโนโลยีสุรนารี
ปีการศึกษา 2564

GLUCOSE CONJUGATED NEAR INFRARED DYES FOR PHOTODYNAMIC
THERAPY IN CANCER CELLS

Suranaree University of Technology has approved this thesis submitted in partial fulfillment of the requirements for a master's degree.

Thesis Examining Committee



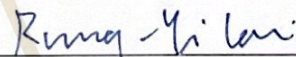
(Prof. Dr. James R. Ketudat-Cairns)

Chairperson



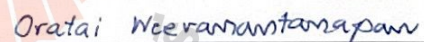
(Asst. Prof. Dr. Anyanee Kamkaew)

Member (Thesis Advisor)



(Dr. Rung-Yi Lai)

Member



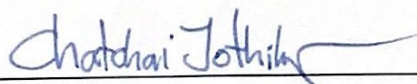
(Asst. Prof. Dr. Oratai Weeranantanapan)

Member



(Dr. Kantapat Chansaenpak)

Member



(Assoc. Prof. Dr. Chatchai Jothityangkoon)

Vice Rector for Academic Affairs

and Quality Assurance



(Prof. Dr. Santi Maensiri)

Dean of Institute of Science

จงจิต ตรีภูล : กลูโคสเชื่อมต่อกับสารเรืองแสงช่วงใกล้อินฟราเรดสำหรับการรักษาโดยใช้แสงเป็นตัวกระตุ้นในเซลล์มะเร็ง (GLUCOSE CONJUGATED NEAR INFRARED DYES FOR PHOTODYNAMIC THERAPY IN CANCER CELLS) อาจารย์ที่ปรึกษา : ผู้ช่วยศาสตราจารย์ ดร. อัญญาณี คำแก้ว, 58 หน้า

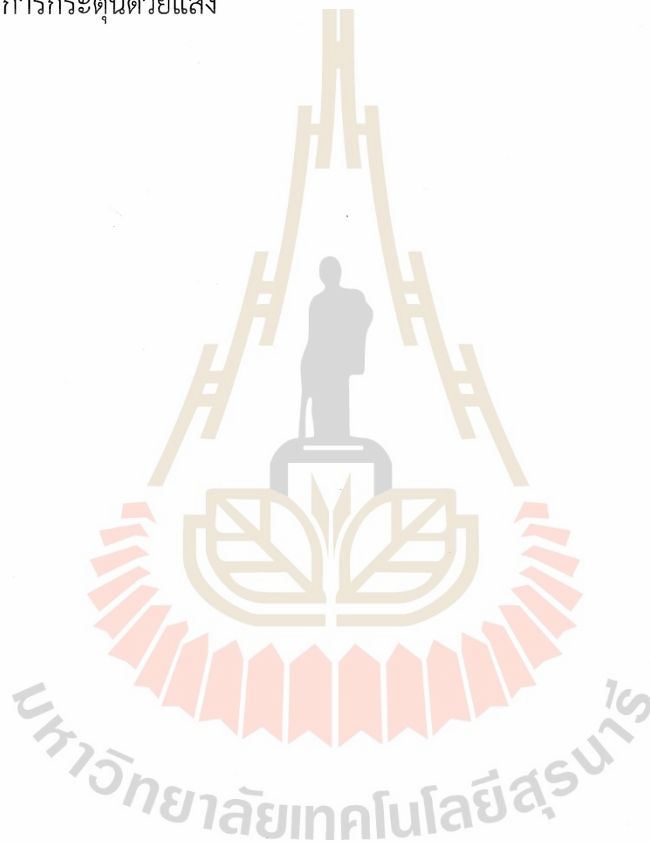
คำสำคัญ: ตัวขนส่งกลูโคส, ผลกระทบของวอร์เบิร์ก, การถ่ายภาพด้วยสารเรืองแสงช่วงใกล้อินฟราเรด การรักษาโดยใช้แสงเป็นตัวกระตุ้น, เอซาบอดีพี

“เซลล์มะเร็งมักจะมีการดูดซึมกลูโคสเพิ่มขึ้นเมื่อเทียบกับเซลล์ปกติ” ข้อความดังกล่าวเป็นส่วนหนึ่งของผลกระทบของวอร์เบิร์ก (Warburg effect) ในการจำแนกมะเร็ง ตามลักษณะเด่นที่โดดเด่นนี้ กลูโคสจึงเป็นลิแกนด์ที่น่าสนใจสำหรับการกำหนดเป้าหมายมะเร็งผ่านตัวขนส่งกลูโคส (Glucose transporters: GLUTs) ที่แสดงออกมากเกินไปในเซลล์มะเร็ง ดังนั้นการศึกษาในครั้งนี้ เราจึงนำเสนอชุดของสารเรืองแสงช่วงใกล้อินฟราเรดของเอซา-บอดีพีที่เชื่อมต่อกับโมเลกุลของกลูโคส (glycoconjugate aza-BODIPY) ได้แก่ AZB-Glc และ AZB-Glc-I ผ่านปฏิกิริยาไฮโคลแอตติชันของเอไซด์-อัลโคน จากการทดลองพบว่าสารเรืองแสง AZB-Glc สามารถใช้เป็นตัวแทนในการถ่ายภาพการเรืองแสงฟลูออเรสเซนซ์สำหรับการวินิจฉัยโรคมะเร็งได้เนื่องจาก AZB-Glc มีความเข้มของการเรืองแสงฟลูออเรสเซนซ์ค่อนข้างสูง ในการทดลองการถ่ายภาพในเซลล์ พบว่าสารเรืองแสง AZB-Glc สามารถผ่านเข้าไปภายในเซลล์มะเร็งเต้านม 2 ชนิดที่มีการแสดงออกของตัวขนส่งกลูโคสที่มากเกินไป ได้แก่ MDA-MB-231 และ MCF-7 มากกว่าเซลล์ไฟโบรบลาสต์ปกติของทารกในครรภ์ของมนุษย์ (HFL1) ซึ่งเป็นเซลล์ปกติ นอกจากนี้น้ำตาลดี-กลูโคส (D-glucose) และคอมเบตาสแตติน (combretastatin) ซึ่งเป็นตัวยับยั้งการเผาผลาญกลูโคส สามารถลดการดูดซึมของสารเรืองแสง AZB-Glc ในเซลล์ในลักษณะที่ขึ้นกับความเข้มข้นของทั้งน้ำตาลดี-กลูโคสและคอมเบตาสแตติน ผลการทดลองนี้ยืนยันว่ากลไกการเข้าสู่เซลล์ของสารเรืองแสง AZB-Glc มีความจำเพาะต่อตัวขนส่งกลูโคส

เพื่อประยุกต์ใช้การเรืองแสงใกล้อินฟราเรดที่เชื่อมต่อกับกลูโคสในการรักษามะเร็งที่เกิดจากการกระตุ้นด้วยแสง (photodynamic therapy) ในการศึกษาครั้งนี้ อะตอมของไอโอดีนถูกเติมลงในโครงสร้างของ AZB-Glc เพื่อเพิ่มประสิทธิภาพการผลิออกซิเจนเชิงเดี่ยวในการทำลายเซลล์มะเร็ง ผลการวิจัยพบว่าเซลล์มะเร็งที่บ่มด้วย AZB-Glc-I ถูกทำลายอย่างมีนัยสำคัญหลังจากการฉายแสงในช่วงใกล้อินฟราเรด และเซลล์มะเร็งดังกล่าวได้รับความเสียหายมากขึ้นเมื่อเพิ่มความเข้มข้นของ AZB-Glc-I และเวลาในการฉายแสง โดยมีค่าความเข้มข้นที่มีผลต่อการยับยั้งการเพิ่มจำนวนของเซลล์ร้อยละ 50 (IC₅₀) เท่ากับ 1.4 ถึง 1.6 ไมโครโมลาร์หลังจากการฉายแสง 1 นาที ซึ่งต่ำกว่าเซลล์

ปกติเกือบ 20 เท่า (IC_{50} เท่ากับ 32 ไมโครโมลาร์) ในทางตรงข้ามพบว่าการรอดชีวิตของเซลล์มะเร็ง อยู่ในระดับสูงเมื่อไม่ถูกฉายแสง (IC_{50} มากกว่า 100 ไมโครโมลาร์) นอกจากนี้พบว่า AZB-Glc-I สามารถผลิตออกซิเจนเดี่ยวภายในเซลล์มะเร็งหลังจากการฉายแสงในช่วงใกล้อินฟราเรด และเซลล์มะเร็งถูกทำลายอย่างสมบูรณ์แม้ใช้ความเข้มข้นของ AZB-Glc-I ในปริมาณต่ำ (2.5 ไมโครโมลาร์)

ในงานวิจัยนี้ผู้วิจัยได้แสดงให้เห็นว่าสารเรืองแสงช่วงใกล้อินฟราเรดของเอซา-บอดีที่เชื่อมต่อกับโมเลกุลของกลูโคสสามารถกำหนดเป้าหมายเซลล์มะเร็งอย่างมีประสิทธิภาพและสามารถใช้ในการบำบัดมะเร็งด้วยการกระตุ้นด้วยแสง



สาขาวิชาเคมี

ปีการศึกษา 2564

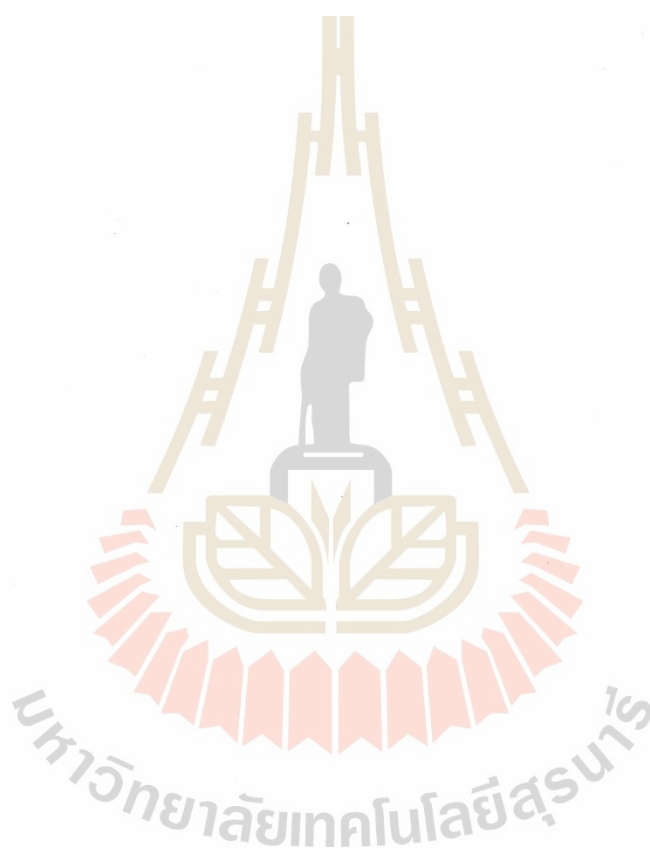
ลายมือชื่อนักศึกษา จวิต ตรีคุณ
ลายมือชื่ออาจารย์ที่ปรึกษา อน

JONGJIT TREEKOON : GLUCOSE CONJUGATED NEAR INFRARED DYES FOR PHOTODYNAMIC THERAPY IN CANCER CELLS. THESIS ADVISOR : ASST. PROF. ANYANEE KAMKAEW, PH.D. 58 PP.

Keywords: Glucose Transporter, Warburg effect, NIR fluorescence imaging, Photodynamic therapy, Aza-BODIPY

As part of the Warburg effect, cancer cells typically have a higher glucose consumption than normal cells. To classify cancer according to this distinctive hallmark, glucose is an attractive ligand for cancer targeting via overexpressed glucose transporters (GLUTs) in cancer cells. In this study, we prepared a series of novel glycoconjugate aza-BODIPY dyes, **AZB-Glc** and **AZB-Glc-I**, by conjugating two glucose moieties to near-infrared dyes through the azide-alkyne cycloaddition reaction. **AZB-Glc** could be used as a fluorescence imaging agent for cancer diagnostics due to its high fluorescence intensity. **AZB-Glc** could be internalized inside GLUTs-overexpressing breast cancer cell lines for cellular imaging, including MDA-MB-231 and MCF-7, to a greater extent than normal cells (human fetal lung fibroblast, HFL1), indicating that the cellular uptake of the probe was correlated with GLUTs. Furthermore, D-glucose and a glucose metabolism suppressor, combretastatin could reduce the cellular uptake of **AZB-Glc** in a dose-dependent manner, demonstrating that this probe uptake mechanism is GLUT-dependent. To widen its usage in cancer treatment, iodine atoms were added to **AZB-Glc** (**AZB-Glc-I**) for improving the effectiveness of light-triggered cell death through photodynamic therapy. After being exposed to NIR light, the cancer cells were intensively reduced by increasing the dose of **AZB-Glc-I** and exposure times. Moreover, **AZB-Glc-I** generated considerable NIR light-induced cytotoxicity ($IC_{50} = 1.4-1.6 \mu M$ after 1 minute of irradiation), which was nearly 20 times lower than that in normal cells ($IC_{50} = 32 \mu M$). All cell lines maintained high cell viability in the dark ($IC_{50} > 100 \mu M$). Furthermore, **AZB-Glc-I** produced singlet oxygen inside cancer cells after NIR irradiation, and the cancer cell was completely killed even with a low dose of the probe ($2.5 \mu M$). Consequently, our glucose conjugated systems have been

demonstrated that they effectively target cancer cells with improving photodynamic cancer therapy.



School of Chemistry

Academic Year 2021

Student's Signature Jongjit Treekoon

Advisor's Signature 

ACKNOWLEDGEMENTS

First and foremost, I want to express my gratitude to my adviser, Asst. Prof. Anyanee Kamkaew, has provided me with vital knowledge and teachings that have guided me through the entire study. I also admire her patience with me, because when we first met, I was a freshman who had no idea how to conduct an experiment, prepare a presentation, or write research papers. She assisted me in dealing with that issue in a variety of ways, including revising my writing, making suggestions, and guiding me when I felt stuck in my work. In addition to the thesis guidance, she also gave me the opportunity to do research projects abroad. This gave me a lot of research ideas and inspired me to pursue my Ph.D. study abroad. Without her kindness, this thesis would not be accomplished, and I could say that she is the best advisor ever.

Next, I would like to thank Prof. Dr. James R. Ketudat-Cairns for providing me with 1-Azido-D-glucopyranose, an important chemical, as well as a lot of helpful advice, suggestions, and discussion during this research. He was the key person in helping me succeed in my research. This research output probably would not have happened without him.

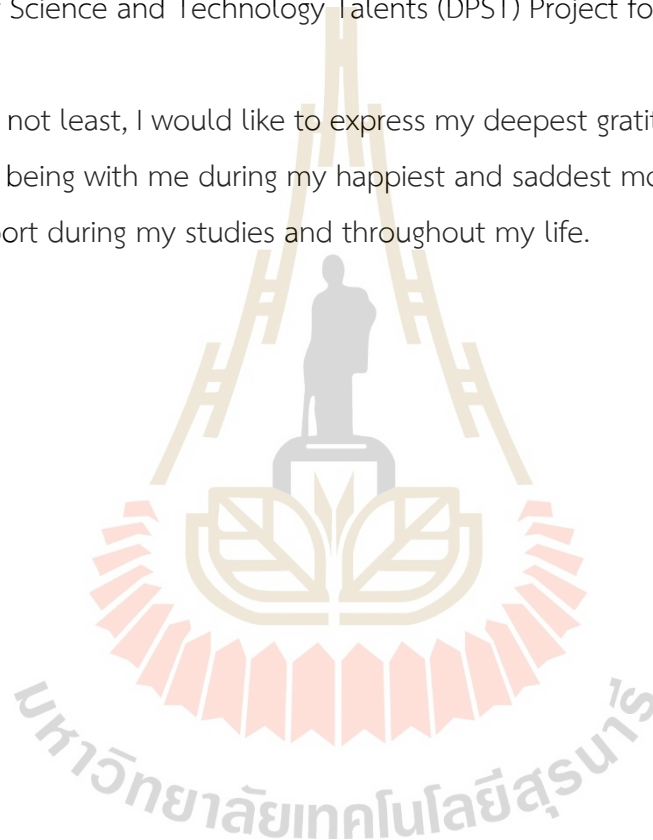
Importantly, I would not be able to complete this thesis without the assistance of Dr. Kantapat Chansaenpak, a researcher at the National Nanotechnology Center (NANOTEC), who accompanied me through all the optical properties experiments and provided helpful advice for all my doubts and questions.

Furthermore, I would like to express my appreciation to my friend and labmate, Thitima Peawklang, who operated and edited some experiments when I went overseas. She gave me a lot of helpful assistance and support. This research would not be perfect without her. In addition, I would like to thank all the AK lab members. Their help and kindness support me in a good environment to conduct research. They always helped me in any way they can, and I can see that they were eager to assist me whenever I asked for it. They provide me with useful advice on how to use the advanced equipment, where to find chemicals, how to run reactions, and so on.

My sincere thanks also go to the school of Chemistry at the Suranaree University of Technology (SUT) for their assistance in study and research facilities. In addition, I am grateful to all my instructors at SUT for their supportive attitudes toward expanding my knowledge and motivating me to be a great student. Moreover, I want to thank my classmates for tutoring me in subjects that I do not understand well. Thank you for cheering me up and chilling out with me. Without them, life as a master's student would be extremely stressful. Besides, I would like to thank the Development and Promotion of Science and Technology Talents (DPST) Project for the scholarships and experience.

Last but not least, I would like to express my deepest gratitude to my family and boyfriend for being with me during my happiest and saddest moments. Thank you for all their support during my studies and throughout my life.

Jongjit Treekoon



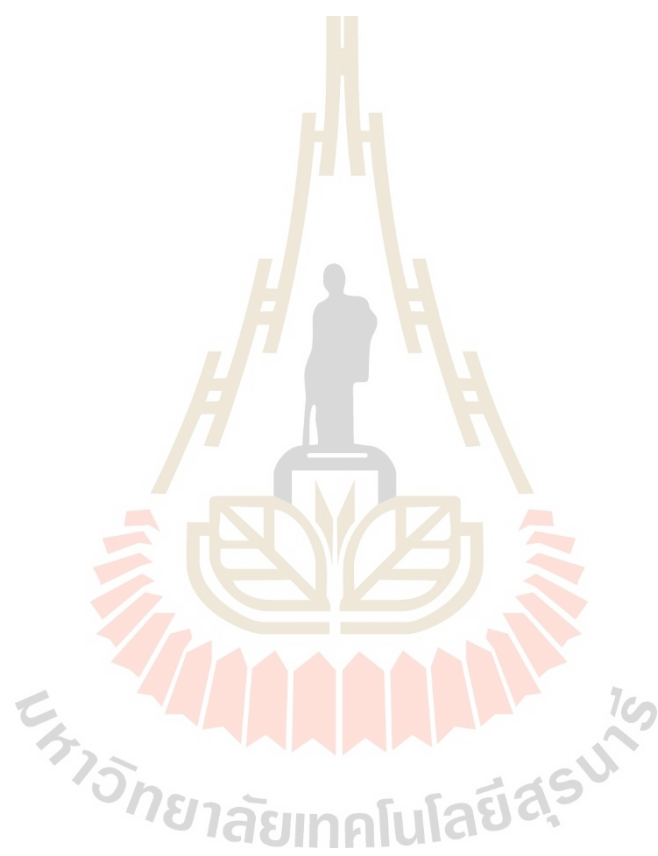
CONTENTS

	Page
ABSTRACT IN THAI.....	II
ABSTRACT IN ENGLISH.....	II
ACKNOWLEDGEMENTS.....	V
TABLE OF CONTENTS.....	VII
LIST OF FIGURES.....	X
LIST OF TABLES.....	XII
LIST OF ABBREVIATIONS.....	XIII
CHAPTER	
I INTRODUCTION.....	1
1.1 Research Background.....	1
1.2 Research Objectives.....	3
CHAPTER	
II LITERATURE REVIEW.....	3
2.1 Overexpression of Glucose Transporters in Breast Cancer Cells.....	4
2.2 Fluorescent Probes for Tumor Diagnosis.....	8
2.3 The First Generation of Fluorescent-Conjugated Glucose probes.....	9
2.4 Near-infrared (NIR) Glucose Conjugated Bioprobs.....	10
2.4.1. The Advantage of Near-infrared (NIR) Bioprobes.....	10
2.4.2 A Review of NIR-Fluorescent Tagged Glucose Analogue for Cancer Cell Imaging and Treatment.....	11
2.5 Halogen-containing aza-BODIPY in Photodynamic (PDT) Therapy.....	16
CHAPTER	
III EXPERIMENTAL SECTION.....	21
3.1 Chemicals.....	21
3.2 Research Design and Methodology.....	23
3.3 General Details for Vis-NIR and Fluorescence Measurements and Quantum Yield Calculations.....	25

CONTENTS (Continued)

3.3.1	Vis-NIR Absorption Measurement	25
3.3.2	Fluorescence Measurement	25
3.4	Singlet-Oxygen Generation Measurements	26
3.5	Cell Experiments	26
3.5.1	Cell Culture.....	26
3.5.2	Cell imaging	26
3.5.3	Co-Localization Analysis	27
3.5.4	<i>D/L</i> -Glucose Competition Test.....	27
3.5.5	Combretastatin Treatment.....	27
3.5.6	Light-Induced Cytotoxicity.....	28
3.5.7	Live/Dead Staining Assay	28
3.5.8	Intracellular Reactive Oxygen Detection	29
3.6	Statistical Analysis.....	29
CHAPTER		
IV	RESEARCH RESULTS.....	30
4.1	Results and Discussion.....	30
4.1.1	Synthesis and Photophysical Properties.....	30
4.1.2	Optical Properties of AZB-Glc and AZB-Glc-I.....	30
4.1.3	Singlet Oxygen Generation Measurement in Vitro of AZB-Glc-I.....	31
4.2	Cell assay	33
4.2.1	Time-Dependent Cellular Uptake of AZB-Glc	34
4.2.2	<i>D/L</i> -Glucose Competition Assay of AZB-Glc	36
4.2.3	Combretastatin Treatment.....	38
4.2.4	Photocytotoxicity Assay of AZB-Glc-I.....	39
4.2.5	Intracellular ¹ O ₂ Detection of AZB-Glc-I.....	41
4.2.6	Live/Dead Viability/Cytotoxicity of AZB-Glc-I	42
CHAPTER		
V	CONCLUSIONS	43
	REFERENCES	46

APPENDIX.....52
CURRICULUM VITAE58

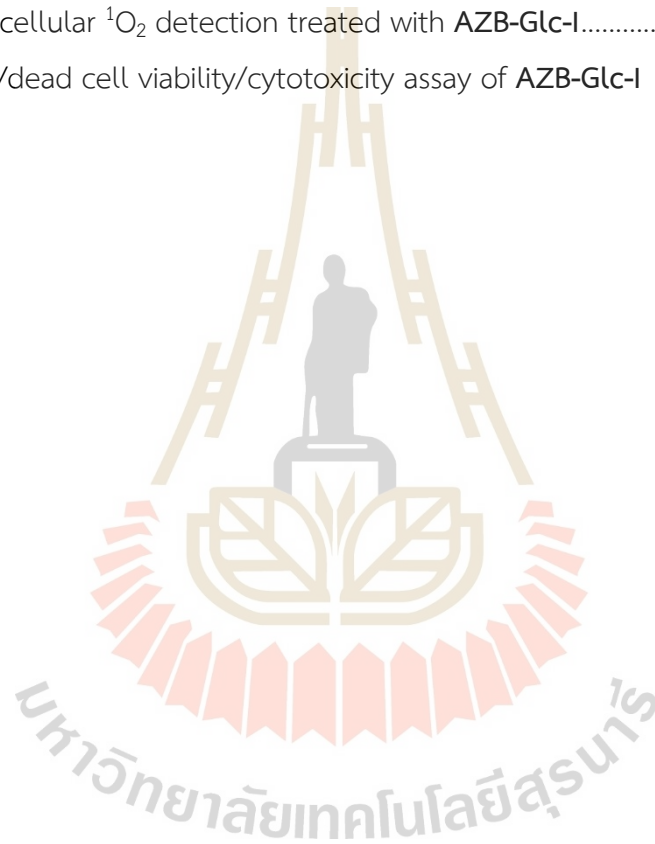


LIST OF FIGURES

Figure		Page
1	Schematic presentation for the overall idea of the Aza-BODIPY-tagged glucose fluorescent probe for photodynamic therapy	2
2	Schematic diagram of glycolysis according to the Warburg effect	4
3	Upregulation of glycolytic metabolism	7
4	Strategies of fluorescent probes for tumor diagnosis.	8
5	Chemical structures of 6-NBDG and 2-NBDG.....	10
6	Penetrability of light through tissue.	11
7	A porphyrin derivative-tagged glucose probe.	12
8	Cyanine-based fluorescent glucose tracer.....	13
9	Silicon rhodamine (SiR)-based fluorescent glucose tracer.....	14
10	Glucose-appended platinum (II)-BODIPY	15
11	Glucose conjugated dicyanoisophorone (DCI) derivatives.	16
12	Jablonski diagram of photodynamic therapy.....	17
13	The modification of the BODIPY core	18
14	Studies of influences of the halogen atom in generating singlet oxygen.....	19
15	Compounds of 2a and 2b.....	20
16	Synthesis of AZB-Glc and AZB-Glc-I	30
17	Absorption and fluorescence spectra of AZB-Glc and AZB-Glc-I	31
18	DPBF absorbance changes at 408 nm	33
19	DPBF absorbance behavior in the presence of AZB-Glc-I	33
20	The first-order kinetic plot of DPBF absorbance	34
21	Time-Dependent Cellular Uptake of AZB-Glc	35
22	Time-Dependent Cellular Uptake of AZB-P	36

LIST OF FIGURES (Continued)

Figure		Page
23	Co-localization experiment in the lysosome of AZB-Glc	36
24	Glucose competition assay between AZB-Glc and D- /L-Glucose	37
25	Glucose competition assay between AZB-P and of D- /L-Glucose	38
26	Confocal imaging of AZB-Glc in breast cancer cells	39
27	Photocytotoxicity experiment by MTT assay of the cells of AZB-Glc-I	40
28	Intracellular $^1\text{O}_2$ detection treated with AZB-Glc-I	42
29	Live/dead cell viability/cytotoxicity assay of AZB-Glc-I	43

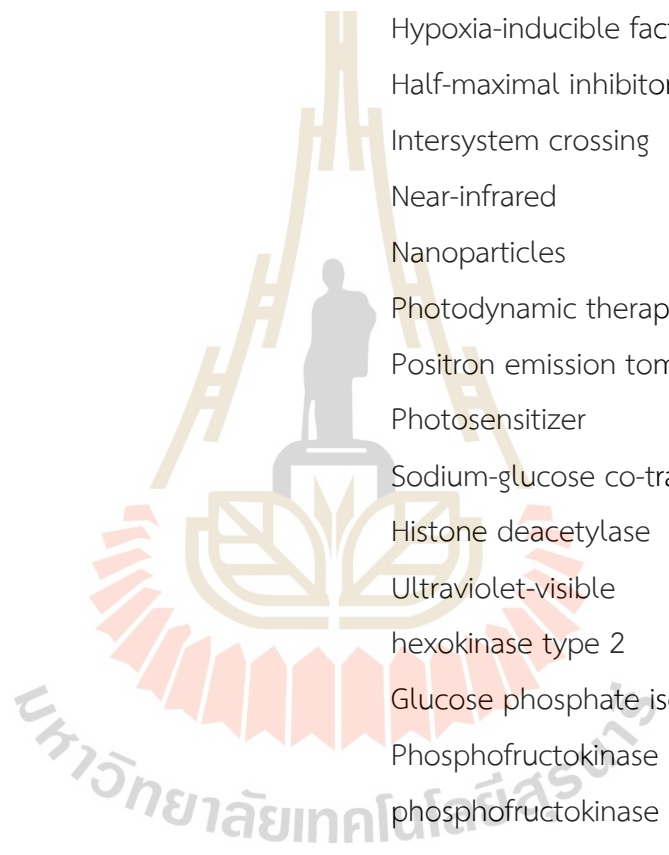


LIST OF TABLES

Table		Page
1	The glucose transporters (GLUTs) families.....	5
2	Chemicals used for the synthesis of the fluorescence probes.....	21
3	Molecular probes for material characterization and cell experiments.....	22
4	Photophysical properties of AZB-Glc and AZB-Glc-I	32
5	The IC_{50} values of AZB-Glc-I in different cell lines.....	41



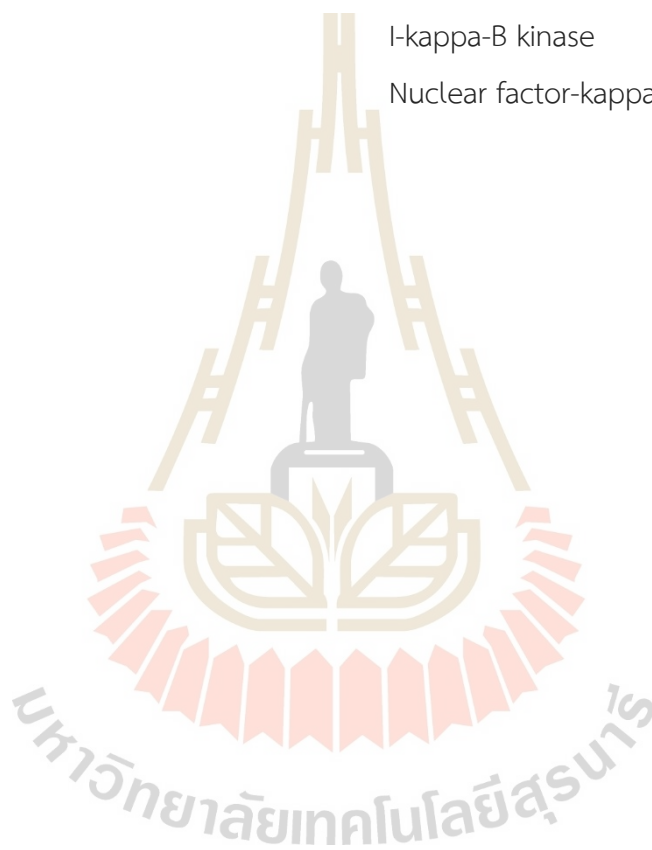
LIST OF ABBREVIATIONS



ATP	Adenosine triphosphate
Aza-BODIPY	Aza-borondipyrromethene
GLUT	Glucose transporter
HIF1	Hypoxia-inducible factor 1
IC ₅₀	Half-maximal inhibitory concentration
ISC	Intersystem crossing
NIR	Near-infrared
NPs	Nanoparticles
PDT	Photodynamic therapy
PET	Positron emission tomography
PS	Photosensitizer
SGLTs	Sodium-glucose co-transporters
SIRT6	Histone deacetylase
UV-Vis	Ultraviolet-visible
HK2	hexokinase type 2
GPI	Glucose phosphate isomerase
PFK1	Phosphofructokinase 1
PFK2	phosphofructokinase 2
ALDA	aldolase A
TPI	Triosephosphate isomerase
GAPDH	Glyceraldehyde 3-phosphate dehydrogenase
PGK1	Phosphoglycerate kinase 1
PGM	Phosphoglycerate mutase
ENO1	Enolase 1
PKM2	Pyruvate kinase type M2

LIST OF ABBREVIATIONS (Continued)

LDH-A	Lactate dehydrogenase type A
PDK1	Pyruvate dehydrogenase kinase-1
TIGAR	TP53-induced glycolysis and apoptosis regulator
SCO2	Synthesis of cytochrome c oxidase2
IKK	I-kappa-B kinase
NFkB	Nuclear factor-kappa-B



CHAPTER I

INTRODUCTION

1.1 Research Background

Photodynamic therapy (PDT) has received a lot of attention in the last decade for cancer treatment since it is a minimally invasive technology that can selectively target tumor cells while having fewer side effects than traditional treatments (Patrizia Agostinis et al., 2011; Allison and Moghissi, 2013; Yano et al., 2011). In PDT, photosensitizers can produce reactive oxygen species (ROS) that are known to oxidize biological substrates in cancer cells, leading to apoptosis or necrosis of these cells when exposed to a specific wavelength of light (Bacellar, Tsubone, Pavani, and Baptista, 2015). An excellent photosensitizer should possess a high fluorescence quantum yield, high photostability, and a long wavelength of light absorption. In this context, near-infrared (NIR) light-absorbing PDT agents are attractive because the light in the 700–1200 nm range can penetrate deep tissue and generate less autofluorescence interference, resulting in a high signal-to-noise ratio in cancer imaging. Moreover, the enhanced selective accumulation in tumors can be obtained by ligand-linked agents, which are widely used for cancer therapy.

Glucose is a key chemical in the creation of intracellular energy in living organisms. Glucose transporters (GLUTs) are a group of membrane proteins that allow glucose to pass across the plasma membrane for cellular glucose uptake. Even under aerobic conditions, cancer cells prefer glycolysis and lactate fermentation to oxidative phosphorylation for maintaining cellular homeostasis, growth, and proliferation, according to the Warburg effect (Warburg, 1956). As a result of the overexpression of GLUTs, cancer cells greatly enhance glucose uptake.

Indeed, 2-deoxy-2-(^{18}F) fluoro-D-glucose (^{18}F -FDG), a radioactive glycoconjugate tracer for positron emission tomography (PET), is widely utilized in clinical practice. However, there are significant disadvantages, including radiation toxicity and long-term

exposure. To avoid this, fluorescence imaging is an alternative way of identifying cancers. A variety of fluorochromes have recently been developed to be glucose bioprobes (Y. Cheng et al., 2020; Fang et al., 2017; Liu et al., 2016; Maric et al., 2019). However, due to the short absorption wavelength (< 700 nm), several probes had limited tissue penetration, and only a few fluorescent glycoconjugates have been reported to harm cancer cells using the PDT (Thomas et al., 2020). Consequently, new NIR glucose conjugated probes are in high demand for cancer treatment combined with diagnosis.

To promote tumor accumulation via glucose uptake channels, an azaborondipyrromethene (Aza-BODIPY) derivative conjugated with glucose moieties were synthesized in this study. Aza-BODIPYs are NIR absorption dyes with strong photostability, simple production, and functionalization. In this investigation, two comparable probes are used: (i) AZB-Glc, which provides imaging-guided to GLUT-overexpressed cancer cells, and (ii) iodinated-AZB-Glc (AZB-Glc-I), which generates large amounts of singlet oxygen for PDT under NIR light irradiation (Figure 1).

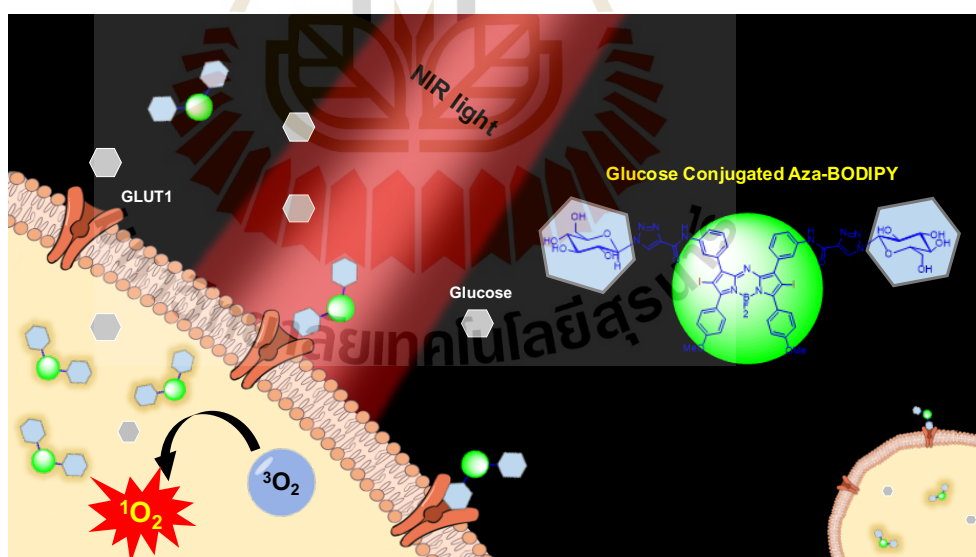


Figure 1 Schematic presentation for the overall idea of the Aza-BODIPY-tagged glucose fluorescent probe (AZB-Glc-I) for photodynamic therapy.

1.2 Research Objectives

This project aims to develop Aza-BODIPY derivatives as a novel NIR glucose conjugated probe to monitor cancers and enhance cancer therapeutic efficacy by PDT. The objectives are the followings.

1) Synthesis and characterization of the glucose-conjugated Aza-BODIPY (**AZB-Glc**) for cellular imaging via GLUT overexpression. This purpose is to design a probe conjugated to glucose molecules that exhibits absorption and fluorescence in the near-infrared (NIR) spectral region. Furthermore, iodinated-AZB-Glc (**AZB-Glc-I**) will be synthesized for improving efficiency in cancer treatment by PDT.

2) To visualize the uptake of **AZB-Glc** *in vitro*. This probe is expected to identify the cancer cells via glucose transporters (GLUTs) using efficient fluorescence imaging.

3) To investigate **AZB-Glc-I** ability as a photosensitizer in PDT. This goal estimated that the **AZB-Glc-I** can generate a high amount of singlet oxygen under red light, demonstrating a significant death of cancer cells in *in vitro* studies.

4) To investigate the utilization of these glucose tracers in cancer cells with highly overexpressed GLUTs, including dark toxicity and another potentially useful medical application. This objective is to confirm the potential of these glucose tracers to continue moving forward to clinical usage.

CHAPTER II

LITERATURE REVIEW

2.1 Overexpression of Glucose Transporters in Breast Cancer Cells

About a century ago, the tumorigenesis phenomenon was reported by the German scientist Otto Warburg, which is known as the Warburg effect or aerobic glycolysis. This effect hypothesized that mitochondria in cancer cells were dysfunctional resulting in higher levels of glycolysis and lactate production than oxidative phosphorylation in the cells, even in the presence of oxygen (Devic, 2016; Warburg, 1956) (Figure 2). Since the irregular metabolism in cancer cells produces less adenosine triphosphate (ATP) per glucose molecule, the cancer cells need a high amount of glucose, an important source of energy for ATP in cells. Therefore, the cells tend to overexpress glucose transporters that promote several biosynthetic pathways (Szablewski, 2013).

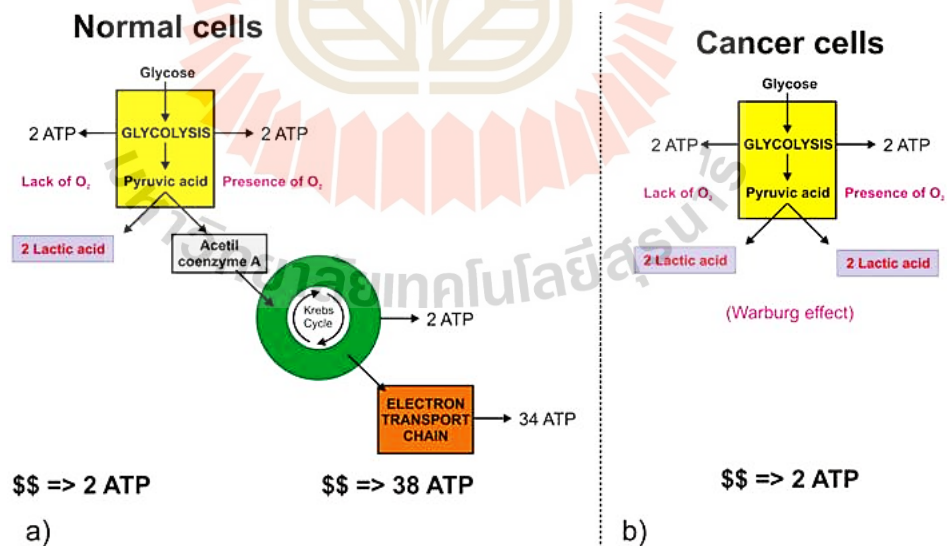


Figure 2 Schematic diagram of glycolysis according to the Warburg effect. Copyright © 2016 Journal of Cancer (Devic, 2016).

In mammalian cells, glucose transporters are classified into two families: sodium-dependent glucose transporters (SGLTs) and facilitative glucose transporters (GLUTs). The SGLT1 and SGLT2 (gene symbol SLC5A) transport glucose with high affinity via a secondary active transport mechanism that transfers glucose into cells using energy from the Na⁺-K⁺ ATPase pump. These transporters have not been reported in the breast cancer (Koepsell, 2017; Lin and Tseng, 2014). The GLUTs family (gene symbol SLC2A) contains 14 membranes: GLUT1-GLUT12, GLUT14, and the H⁺/myo-inositol (HMI) transporter. They exhibit a tissue-specific expression and can be divided into 3 classes (Scheepers, Joost, and Schurmann, 2004) (Table 1).

Table 1 The glucose transporters (GLUTs) families.

Isoform	Class	Main tissue localization
GLUT1	I	Erythrocytes, brain, ubiquitous
GLUT2	I	Liver, pancreas, intestine, kidney
GLUT3	I	Brain
GLUT4	I	Heart, muscle, adipose tissue, brain
GLUT5	II	Intestine, testes, kidney
GLUT6	III	Brain, spleen, leucocytes
GLUT7	II	n.d.
GLUT8	III	Testes, brain, and other tissues
GLUT9	II	Liver, kidney
GLUT10	III	Liver, pancreas
GLUT11	II	Heart, muscle
GLUT12	III	Heart, prostate, muscles, small intestine, adipose tissue
GLUT14	I	Testes
HMIT	III	Brain

Glucose transporters that possess a high affinity for glucose are GLUT1, GLUT3, and GLUT4 (Mueckler and Thorens, 2013). Cellular glucose uptake in tumor cells increases the GLUT transporters, according to the Warburg effect. Overexpression of GLUT1 and/or GLUT3 has been consistently demonstrated as the preeminent event in many types of cancer, including colorectal carcinoma, breast carcinoma, lung

adenocarcinoma, squamous cell carcinoma, ovarian carcinoma, and glioblastoma (Ancey, Contat, and Meylan, 2018; Macheda, Rogers, and Best, 2005; Zambrano, Molt, Uribe, and Salas, 2019). In addition, GLUT1 was found to be overexpressed in breast cancer cell lines (e.g., MCF-7 and MDA-MB-231) (Laudanski, Swiatecka, Kovalchuk, and Wolczynski, 2003). Glucose uptake by GLUT1 affects the early stages of breast cancer by causing changes in the breast epithelial cell metabolism and may be a part of the neoplastic process (Wellberg et al., 2016).

Hypoxia is one of the variables that cause GLUT1 overexpression in breast cancer cells. Hypoxia response elements are found in the promoters of GLUT1 and bind the hypoxia-inducible factor (HIF1) to facilitate transcription. Since an increase in HIF-1 α protein levels is a common occurrence in most malignancies, it provides a biological mechanism for cancer-related GLUT1 overexpression. Besides HIF-1, the histone deacetylase SIRT6, the cellular oncogene product c-MYC (V-Myc Avian Myelocytomatosis Viral Oncogene Homolog), the pro-survival protein kinase Akt (Protein Kinase B), and mutant p53 (Figure 3). All of which can increase the expression and function of proteins involved in energy generation via the glycolytic pathway in cancer cells, such as GLUT1 (Yeung, Pan, and Lee, 2008). In addition, the upregulation of GLUT1 is also induced by the ovarian hormone estrogens in human breast cancer cells (Rivenzon-Segal, Boldin-Adamsky, Seger, Seger, and Degani, 2003). Consequently, glucose transporters are useful in distinguishing cancer cells from healthy cells.

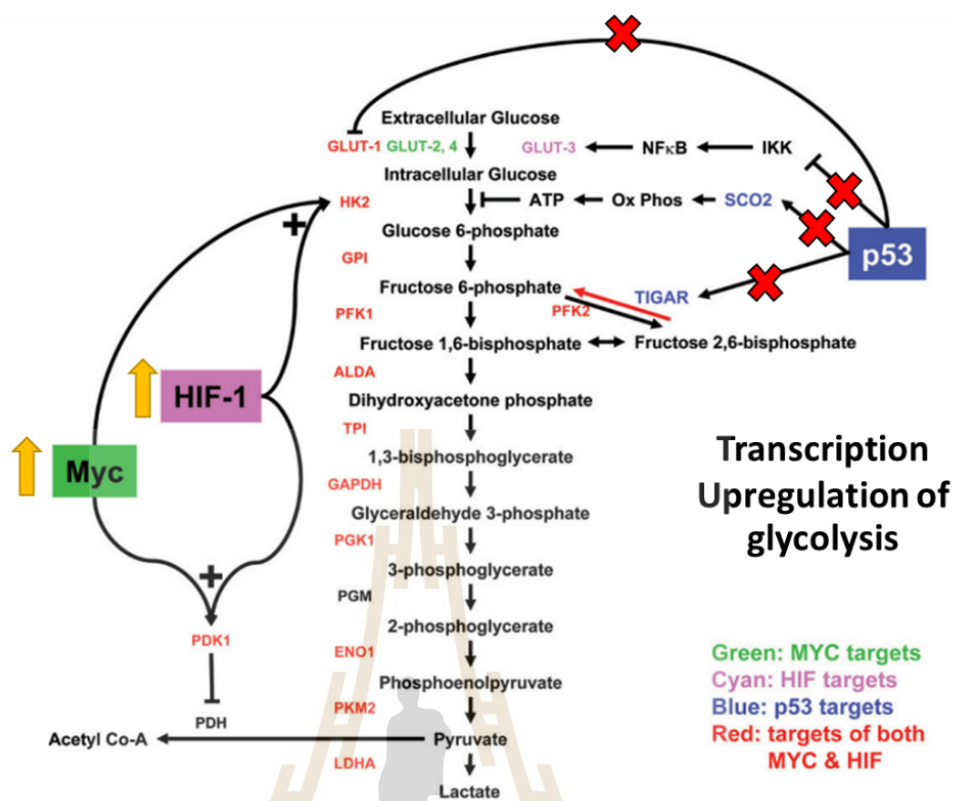


Figure 3 Upregulation of glycolytic metabolism is mainly controlled by c-MYC, HIF-1, and p53. Increased activity of the transcription factors cMYC and HIF-1 in cancer cells leads to overexpression of genes coding for glucose transporters, glycolytic, and regulatory enzymes, as well as a coordinated loss of regulatory proteins due to p53 dysfunction. The loss of p53 function also promotes the NFκB to activate GLUT-3 transcription. p53-controlled genes are in blue fonts, MYC-controlled genes are in green fonts, HIF-1-controlled genes are in cyan fonts, and both HIF-1 and MYC-controlled genes are in red fonts. The arrows signify stimulation/activation, while the ends represent inhibition. Synergism is indicated by a plus sign (+). Abbreviations: see at the list of abbreviations. Copyright © 2008 Springer Nature Switzerland AG (Yeung et al., 2008).

2.2 Fluorescent Probes for Tumor Diagnosis

Fluorescence imaging provides a promising tool for biological research and even for clinical use through real-time and high-resolution imaging. The fluorescence signal can provide information associated with the anatomical structure and metabolism of a tumor, which is helpful for therapeutic planning and injury reduction. Importantly, fluorescence systems need to be stable, efficient, and safe for the achievement of accurate and personalized medicine. A successful fluorescent probe demonstrates several requirements for medical imaging, such as photostability, high fluorescence intensity, specific tissue accumulation, biodegradability, and pharmacokinetics. One approach is to directly conjugate ligands, such as antibodies, proteins, and sugar that are selective to the cell surface receptors, to a fluorescent probe that may be an active or activatable imaging probe (Figure 4) (Gao, Yu, Lv, Choo, and Chen, 2017).

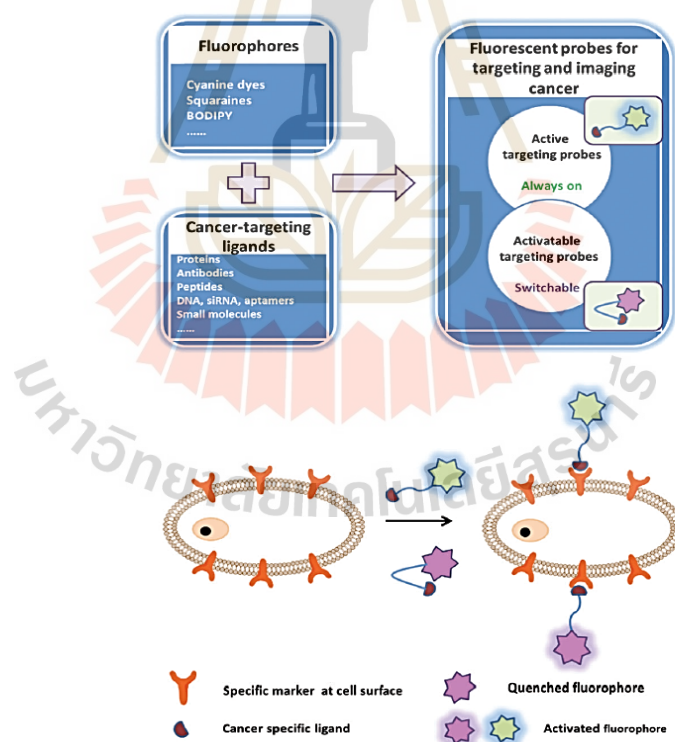


Figure 4 Strategies of fluorescent probes for tumor diagnosis. Copyright © 2017 Royal Society of Chemistry (Gao et al., 2017).

2.3 The First Generation of Fluorescent-Conjugated Glucose probes

Increased glucose uptake by cancer cells has been clinically used in cancer diagnosis and follow-up using a radiolabeled glucose analog in positron emission tomography (PET). [^{18}F]-2-fluoro-2-deoxy-D-glucose, ^{18}F -FDG remains the most commonly used in clinical and preclinical settings. However, the utilization of radiolabeled bio probes is limited for cell imaging because of their radioactivity and unmeasurable issues in living cell lines. (Gambhir, 2002; Kubota, 2001; Yaylali, Kirac, and Yuksel, 2016) In this context, the development of fluorescent glucose tracers has been focused on improving the spatial/temporal resolution for monitoring cellular glucose uptake at the single-cell level. In 1985, A fluorescent glucose analogue, the fluorophore 7-nitrobenz-2-oxa-L,3-diazol-4-yl (NBD) attached to D-glucose moiety (6-NBDG) was first developed to study the human erythrocyte glucose transport through GLUTs by fluorescence imaging (Speizer, Haugland, and Kutchai, 1985). The NBD showed strong green fluorescence (550 nm) for cancer imaging. Furthermore, the phosphorylation of 6-NBDG by the hexokinase enzyme is blocked when the C-6 position of the glucose moiety is conjugated to 6-NBDG, resulting in a buildup of 6-NBDG within the cells. Eleven years after the development of 6-NBDG, 2-(N-(7-nitrobenz-2-oxa-L,3-diazol-4-yl) amino)-2-deoxyglucose (2-NBDG) was synthesized and applied to assess the glucose uptake activity of *Escherichia coli B* and cell metabolic event because the modification at the C-2 position of glucose allows phosphorylation by the glycolytic enzyme, hexokinase. Therefore, 2-NBDG can monitor cell metabolism by degrading the fluorescence (Yoshioka et al., 1996). Both 6-NBDG and 2-NBDG are commonly used to monitor glucose uptake and transport related to GLUTs in a single cell and in real-time. However, because of their low sensitivity and restricted tissue penetration due to their short absorbance wavelength, the NBDGs are not an acceptable bioprobe for *in vivo* glucose uptake monitoring (Figure 5).

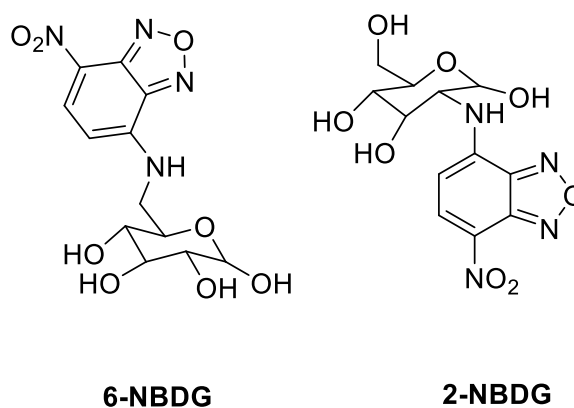


Figure 5 Chemical structures of 6-NBDG and 2-NBDG.

2.4 Near-infrared (NIR) Glucose Conjugated Bioprobes

2.4.1 The Advantage of Near-infrared (NIR) Bioprobes

Near-infrared (NIR) fluorescent probes with absorption wavelengths between 600 and 900 nm (deep red to NIR) have been recently developed for cancer monitoring by modifying the probes to have good hydrophilicity, high photostability, high fluorescent quantum yield, and excellent contrast in biological systems (Escobedo, Rusin, Lim, and Strongin, 2010; X. Zhang, Bloch, Akers, and Achilefu, 2012). In addition, NIR probes are preferable for *in vivo* fluorescence applications because of the minimal absorption and light scattering of NIR light by biological chromophores such as proteins, nucleic acids, hemoglobin, and melanin in tissues, providing for deep tissue penetration and a high signal-to-background ratio. (Dąbrowski et al., 2016; Zhou, Song, Nie, and Chen, 2016) (Figure 6).

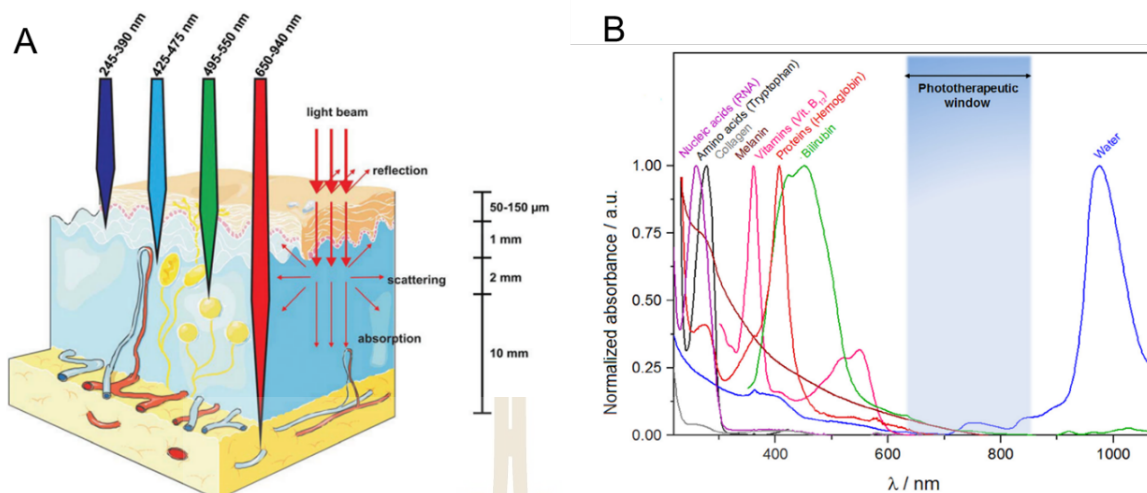


Figure 6 Penetrability of light through tissue. Different wavelengths can penetrate different layers of tissue depending on their absorption, scattering, transmission, and reflection by the tissue (A). Copyright © 2016, Royal Society of Chemistry (Zhou et al., 2016). The spectral region of visible and NIR light (650–850 nm). The light in this region is known as the phototherapeutic window that is not disturbed by other biomolecules, leading to a high signal-to-noise ratio (B). Copyright © 2016 Elsevier B.V. (Dąbrowski et al., 2016).

2.4.2 A Review of NIR-Fluorescent Tagged Glucose Analogue for Cancer Cell Imaging and Treatment.

Recently, developments of cyanine, rhodamine, porphyrin derivatives, and BODIPY glucose analogs can be good candidates for glucose transporter-mediated bioimaging and cancer therapy.

In 2003, Pyropheophorbide 2-deoxyglucosamide (Pyro-2DG), The development of Pyro-2DG is the beginning of the alternative fluorescent-tagged glucose. The Pyro-2DG contains a porphyrin derivative, which is a NIR fluorescent dye. In addition to being used as a fluorescence probe for cancer detection, NIR dyes have the potential to photosensitize cancer cells for treatment with photodynamic therapy (PDT). Confocal microscopy images suggested that Pyro-2DG was highly accumulated in the 9L glioma-bearing animal compared to surrounding normal tissue such as muscle. In addition, the red fluorescent of Pyro-2DG decreased under the presence of 50 mM D-glucose in

the 9L glioma cell line, indicating the specificity of Pyro-2DG toward the GLUT/hexokinase pathway. Under the PDT, the Pyro-2DG could damage mitochondrial in the region of the tumor after injection of the agents via the tail vein of the rat. This demonstrated that Pyro-2DG had localized to the tumors and caused tumor destruction under photoirradiation (Figure 7) (M. Zhang et al., 2003).

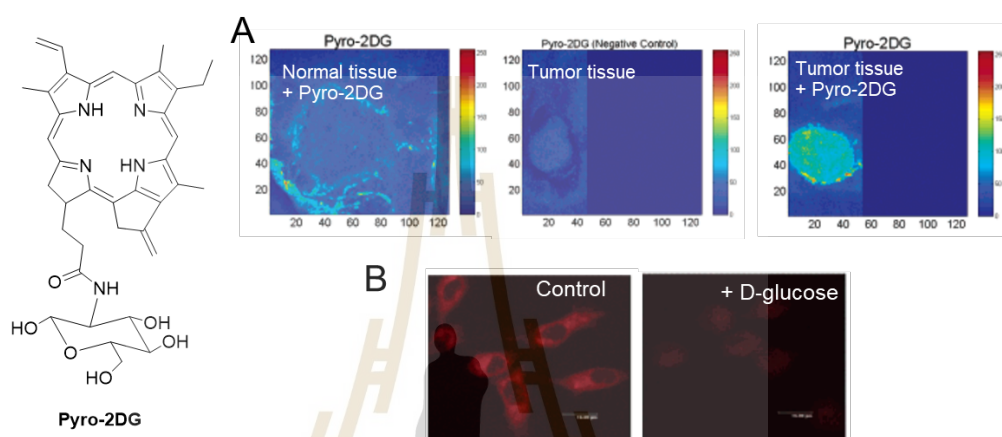


Figure 7 Pyro-2DG, a porphyrin derivative -tagged glucose probe. (A) Fluorescence images of Pyro-2DG in the 9L glioma-bearing animal. (B) The competition assay between Pyro-2DG (50 μM) and D-glucose (50 μM) in 9L glioma cells for 30 min. Copyright © 2003 American Chemical Society (M. Zhang et al., 2003).

Several cyanine-based fluorescent compounds, including Cy5.5-D-glucosamine (Cy5.5-2DG), CyNE 2-DG, and IRDye800CW 2-DG, are glucose tracers with high stability, fluorescence intensity, biocompatibility, and sensitivity in labeling cancer cells (Z. Cheng et al., 2006; Kovar, Volcheck, Sevick-Muraca, Simpson, and Olive, 2009; Lee, Lee, Park, and Park, 2011; Vendrell, Samanta, Yun, and Chang, 2011). In 2014, Seung Bum Park et al. demonstrated the glucose bioprobe Cy3 derivative for targeting the GLUTs and applying the studies of fluorescence imaging to a zebrafish model. As a result, the fluorescent signal of GB2-Cy3 can be seen in zebrafish larval eyes at a dose of 2 μM , and the signal steadily increases as the dye concentration increases up to 80 M, with a greater signal to noise ratio than 2-NBDG. Besides, The GB2- Cy3 uptake can be distinctly reduced in zebrafish larval eyes in the presence of 30 mM of D-glucose and

fluorescence signal in a dose-dependent manner but had no effect on L-glucose. This observation suggested that Glc-SiR-CO₂H cellular uptake is primarily GLUT-dependent, which is important for monitoring glucose uptake in living cells (Figure 9) (Jo et al., 2018).

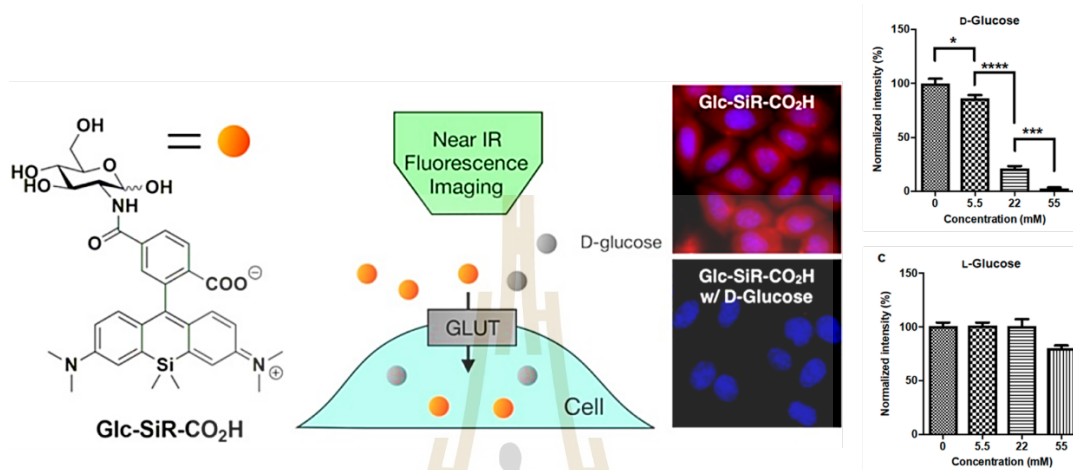


Figure 9 Glc-SiR-CO₂H, silicon rhodamine (SiR)-based fluorescent glucose tracer. Schematic representation of the main idea of the Glc-SiR-CO₂H, which can internalize into cancer cells via GLUTs. The cellular uptake of Glc-SiR-CO₂H can be inhibited by D-glucose in dose-dependent manners, but not influenced by L-glucose. Scale bar = 10 μ m. Copyright © 2018 Royal Society of Chemistry (Jo et al., 2018).

[Pt(L2) (R-BODIPY)] Cl, 2), a platinum (II)-based BODIPY with an appended glucose moiety, was also developed for enhanced NIR cellular imaging-guided PDT. This complex 2 had an absorption wavelength of 715 nm ($3.2 \times 10^4 \text{ M}^{-1} \text{ cm}^{-1}$) in 10% dimethyl sulfoxide (DMSO)- Dulbecco's Modified Eagle's Medium (DMEM) (pH 7.2). Moreover, complex 2 can generate singlet oxygen (¹O₂) in red light, which exhibited a ¹O₂ oxygen quantum yield of 0.6. The photodynamic ability test revealed that red light-induced cytotoxicity of complex 2 in HeLa cervical cancer, HeLa lung cancer, and MCF-7 breast cancer cells (IC₅₀: 2.3-24.7 μ M in light) with negligible dark toxicity (IC₅₀ > 100 μ M). Furthermore, the JC-1 assay revealed that complex 2 was strongly localized in the mitochondria (Figure 10) (Ramu, Gautam, Garai, Kondaiah, and Chakravarty, 2018).

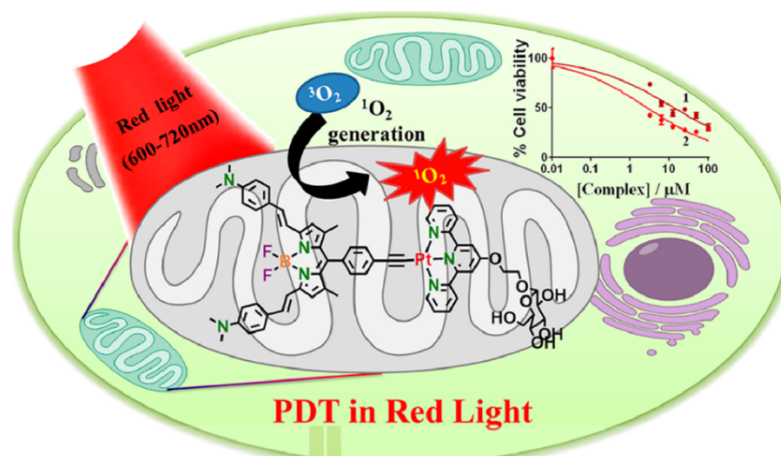


Figure 10 Pt(L2) (R-BODIPY)] Cl, 2, glucose-Appended Platinum (II)-BODIPY. The main idea of the Pt(L2) (R-BODIPY)] Cl, 2 that can be specific with GLUTs and demonstrates mitochondrial localization of the complexes is depicted schematically. This complex also creates singlet oxygen for PDT cancer therapy when exposed to red light. Copyright © 2018 American Chemical Society.

In 2019, Enmin Li et al. synthesized electron donor-acceptor (D–A) structures based on dicyanoisophorone (DCI) derivatives conjugated to the C-1 position of D-glucose (Glu-1-O-DCSN). This probe showed a deep-red emission with a large stoke shift up to 140 nm (λ_{ex} at 530 nm). Glu-1-O-DCSN exhibited good competition with D-glucose for internalization in GLUT1-overexpressed KYSE150 cells. The bioimaging of Glu-1-O-DCSN *in vivo* was investigated further by injecting the probe intravenously into the KYSE150-tumor-bearing mouse. Figure 11 shows that 6 hours after injection, a strong fluorescent signal was seen in the tumor, demonstrating that Glu-1-O-DCSN could target mediated tumor cells, likely by GLUT1. In addition, some of the probes remained in the brain and the liver, which indicates that the probes could cross the Blood-Brain Barrier (BBB), which is a possible application in tumor and brain disease imaging (Figure 11) (Y. Cheng et al., 2020).

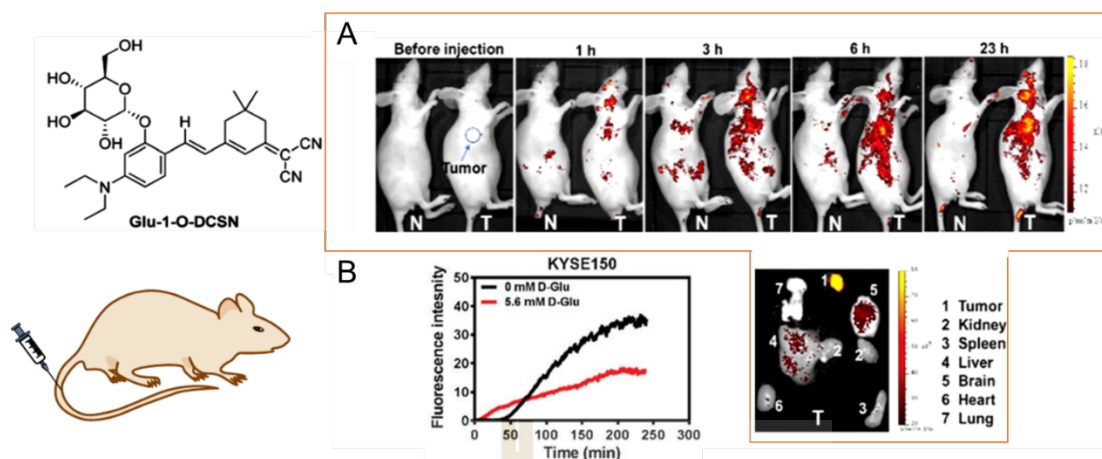


Figure 11 Glu-1-O-DCSN, glucose conjugated dicyanoisophorone (DCI) derivatives. A) Bioimaging in KYSE150-Tumor-Bearing Mouse in the whole body and main organs after injection of Glu-1-O-DCSN. B) Real-time monitoring cellular uptake of Glu-1-O-DCSN before and after in the presence of D-glucose (5.6 mM). Copyright © 2020 Royal Society of Chemistry (Y. Cheng et al., 2020).

2.5 Halogen-containing aza-BODIPY in Photodynamic (PDT) Therapy

Photodynamic (PDT) therapy is a promising anti-tumor strategy and is a minimally invasive method compared to the traditional method for cancer therapy and widely used in clinical trials (Huang, 2005; van Straten, Mashayekhi, de Bruijn, Oliveira, and Robinson, 2017). Applications of PDT require three key components: light, oxygen, and a light activatable molecule, or photosensitizer (PS). When PSs are exposed to light, electrons in the ground state of PSs are stimulated into a higher energy state (S_0 to S_n). This excited PS is unstable and releases this excess energy into fluorescence and/or heat by the internal conversion process. Alternatively, the electrons in the excited singlet state can undergo intersystem crossing into the triplet state (T_1) with the inverted spin of the electron. The electron from the triplet state can disintegrate the radiation transfer electron to create radicals through type 1 reactions or occur in type 2 reactions that tend to transfer some energy to oxygen molecules (3O_2) to form single oxygen (1O_2), which are toxic substances involved in PDT (Figure 12). 1O_2 generation damages cell macromolecules irreversibly, resulting in tumor cell death by apoptotic, necrotic, or autophagic pathways (P. Agostinis et al., 2011).

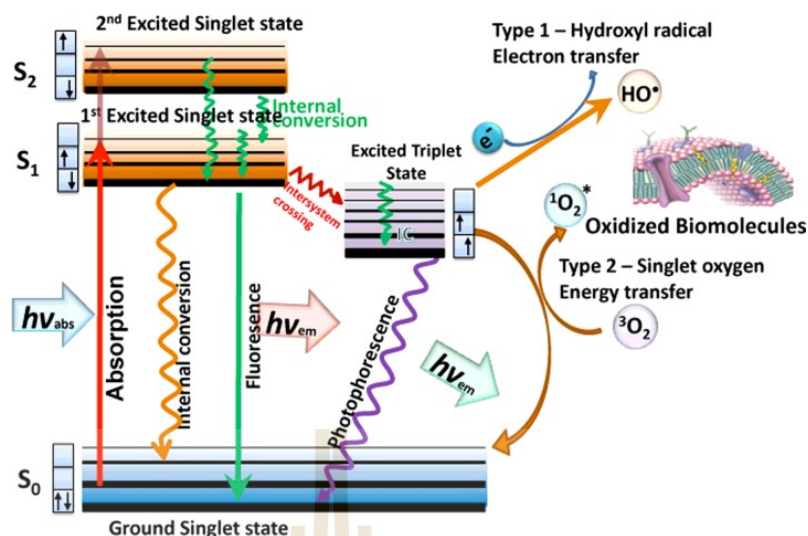


Figure 12 Jablonski diagram of photodynamic therapy. The electron is excited triplet state can transfer energy to intracellular oxygen molecules, resulting in singlet oxygen generation, which can be used to oxidize most biomolecules such as proteins, lipids, and nucleic acids. On the other hand, the electron in the excited triplet state can transfer to water to create the hydroxy radical. Copyright © 2015 American Chemical Society (Bacellar et al., 2015).

Dipyromethene boron difluoride (difluoroboradiaza-*s*-indacene, BODIPY) dye is well known to be used as a photosensitizer for PDT (Kamkaew et al., 2013; Kue et al., 2018). However, its low fluorescence intensity, low 1O_2 generation, and short absorbance wavelength are limited to treating superficial wounds only. These limitations can be overcome by using Aza-BODIPY, in which the meso-carbon of the BODIPY is substituted by nitrogen (Figure 13) (Ge and O'Shea, 2016; Sola and Bañuelos-Prieto, 2019).

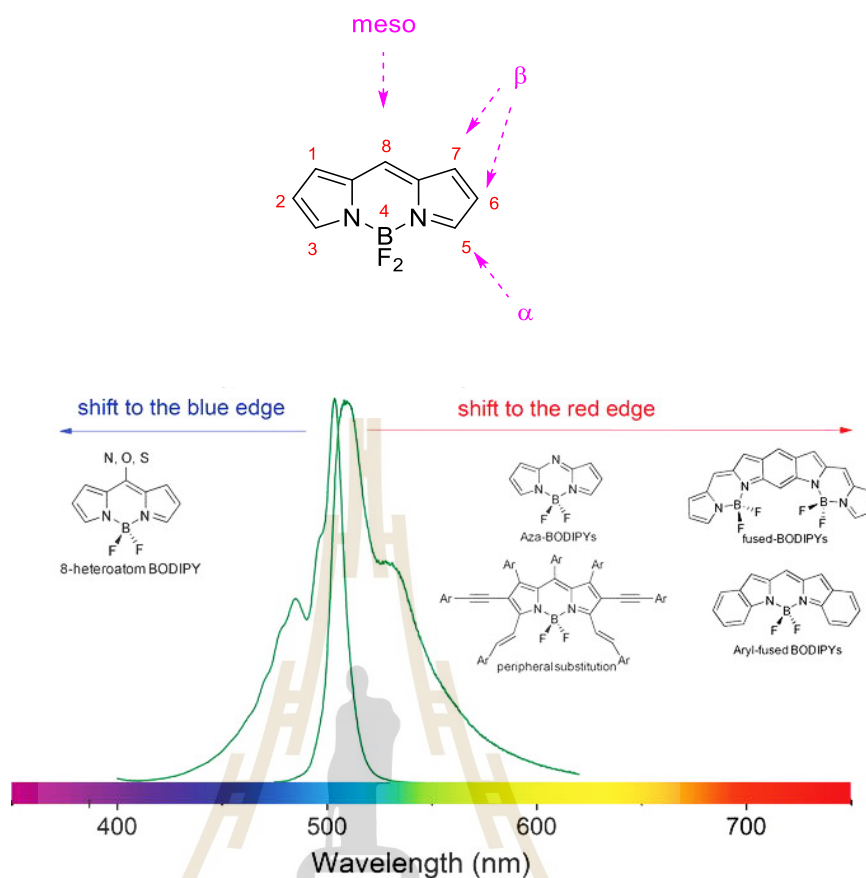


Figure 13 The modification of the BODIPY core for extending the absorption wavelength. Copyright © 2019 IntechOpen (Sola and Bañuelos-Prieto, 2019).

The photosensitizer must be capable of producing $^1\text{O}_2$ from T1; in fact, most BODIPY dyes can be efficiently excited into higher-level singlet states without crossing to triplet states, resulting in low $^1\text{O}_2$ generation. This problem can be overcome by attaching heavy atoms to the core structure of the dyes, which enhances Spin-orbit coupling and thus facilitates the intersystem crossing (ISC) efficiency to promote $^1\text{O}_2$ quantum yields. However, fluorescence emission is frequently reduced (De Simone, Mazzone, Pirillo, Russo, and Sicilia, 2017; Gorman et al., 2004). It is noteworthy that metal-based compounds are difficult to eliminate from the body and leave residues behind (Egorova and Ananikov, 2017; Ndagi, Mhlongo, and Soliman, 2017). Therefore, the most frequently encountered method is halogenation. In 2018, Qiang Zhao et al. studied the influence of halogen atoms attached to Aza-BODIPY for singlet oxygen generation ability, including iodine, bromine, and chloride. This work used DPBF as a

$^1\text{O}_2$ scavenger, the DPBF reacts with $^1\text{O}_2$ to form an unstable peroxide that decomposes into a colorless compound, indicating the formation of singlet oxygen. The absorbance of DPBF in the di-iodinated-Aza-BODIPY B4 condition declined more than the absorbance of other probes under NIR light. The results suggested that the iodine atom had the most impact on the generation of singlet oxygen by PDT. This phenomenon can be explained by the “heavy atom effect” as mentioned before (Figure 14)(Zhao et al., 2018).

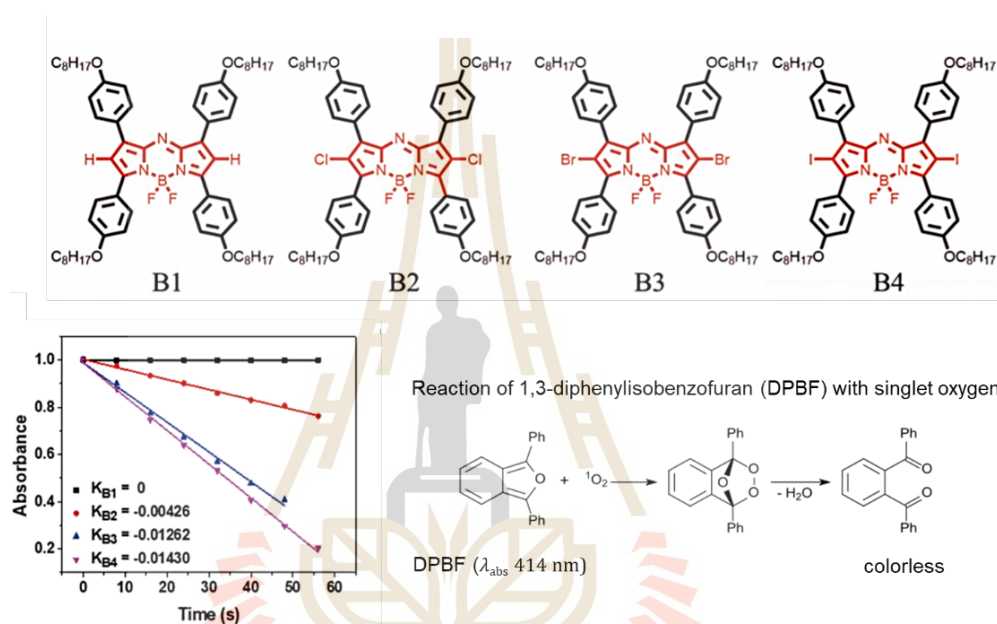


Figure 14 Studies of influences of the halogen atom in generating singlet oxygen of Aza-BODIPY compounds. This experiment used DPBF as a $^1\text{O}_2$ scavenger for measurement. Copyright © 2018 John Wiley and Sons, Inc (Zhao et al., 2018).

In addition, the amount of iodine in the structure has affected the efficiency of PDT. Dong and co-workers created a series of halogenated BODIPY 2a and 2b (Figure 8). They found that 2a with two I atoms exhibited $^1\text{O}_2$ quantum yields (Φ_f) equal to 73%, which is higher than that of 2b (68 %) with four I atoms. In HeLa cells, 2a showed the lowest half-maximal inhibitory concentration (IC_{50}) of only $1.0 \mu\text{M}$, whereas 2b had IC_{50} values of $2.8 \mu\text{M}$. This can be concluded that adding two extra heavy atoms is insufficient to increase the $^1\text{O}_2$ quantum yields. The MTT assay showed that 2b nanoparticles (NPs) have substantially higher dark toxicity than 2a NPs, but lower

phototoxicity than 2a NPs (Figure 15). In addition, an *in vivo* investigation indicated that 2a NPs showed strong phototoxicity, low dark toxicity, and good biocompatibility (Zou et al., 2017).

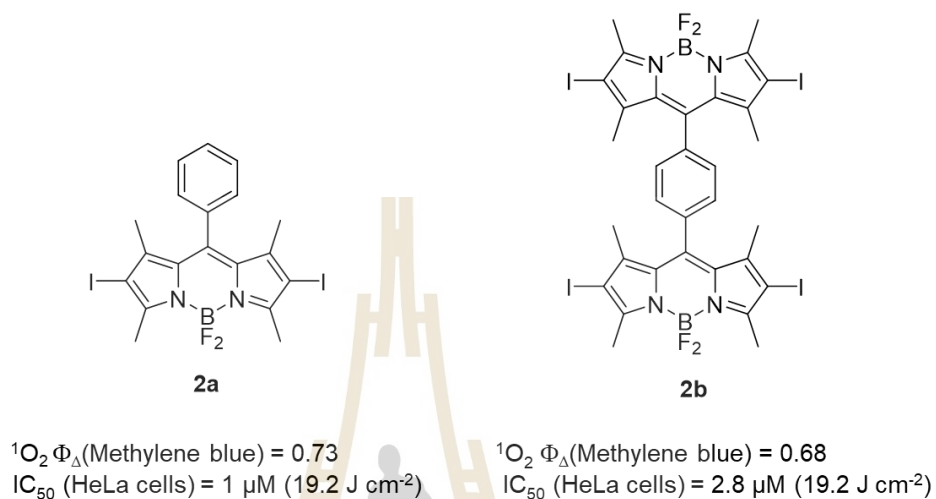


Figure 15 Compounds of 2a and 2b.

This study will employ the Di-iodinated-Aza-BODIPY derivative in imaging-guided photodynamic therapy to kill cancer cells. In addition, an electron-donating group (such as -OMe) will be added to the para-relational with the alkene to expand electron conjugation in the complex, resulting in longer NIR absorption wavelengths. *In in vitro* experiments, the Aza-BODIPY derivative will be conjugated with a glucose moiety to discriminate cancer cells from normal cells. This probe will then tend to localize into cancer cells via glucose transporters (GLUTs).

CHAPTER III

EXPERIMENTAL SECTION

3.1 Chemicals

AZB-NH₂ and AZB-P were synthesized according to the literature procedure. (Kamkaew and Burgess, 2015; Pewklang, Chansaenpak, Lai, Noisa, and Kamkaew, 2019) 1-Azido β-D-glucopyranose was prepared according to the previous protocol (Gorantla et al., 2019). All solvents and reagents were obtained from commercial sources and used without extra purification. The chemicals and solvents used in this research as shown in Table 2 and Table 3.

Table 2 Chemicals used for the synthesis of the fluorescence probes.

Chemicals names	Chemical formular	Sources
Sodium ascorbate	C ₆ H ₇ NaO ₆	TCI
Copper (II) sulfate pentahydrate	CuSO ₄ ·5H ₂ O	Carlo Erba
Ethyl acetate	C ₄ H ₈ O ₂	Sigma-Addrich
Dimethyl sulfoxide (DMSO)	C ₂ H ₆ OS	Sigma-Addrich
Diethyl ether	(C ₂ H ₅) ₂ O	Sigma-Addrich
Hexane	C ₆ H ₁₄	Sigma-Addrich
N-Iodosuccinimide	C ₄ H ₄ INO ₂	TCI
Chloroform	CHCl ₃	Sigma-Addrich
Acetic acid	CH ₃ COOH	Sigma-Addrich
Sodium bicarbonate	NaHCO ₃	TCI
Sodium thiosulfate	Na ₂ S ₂ O ₃	TCI
Ethanol	C ₂ H ₅ OH	Sigma-Addrich

Table 3 Molecular probes for material characterization and cell experiments.

Chemicals names	Chemical formular	Sources
1,3-diphenylisobenzofuran (DPBF)	C ₂₀ H ₁₄ O	Sigma-Addrich
<i>D</i> -Glucose	C ₆ H ₁₂ O ₆	Thermo Fisher
<i>L</i> -Glucose	C ₆ H ₁₂ O ₆	Sigma-Addrich
Methyl thiazolyl tetrazolium (MTT)	C ₅ H ₆ N ₅ S	Sigma-Addrich
Combretastatin	C ₁₈ H ₂₂ O ₆	Sigma-Addrich
Hoechst 33342	C ₂₇ H ₂₈ N ₆ O	Thermo Fisher
Calcein acetoxymethyl (Calcein-AM)	C ₄₆ H ₄₆ N ₂ O ₂₃	Thermo Fisher
Propidium iodide (PI)	C ₂₇ H ₃₄ N ₄	Thermo Fisher
2,7-dichloro-dihydro-fluorescein diacetate (DCFH-DA)	C ₂₄ H ₁₆ Cl ₂ O ₇	Sigma-Addrich

Reactions were monitored by TLC Silica gel 60 F254 (Merck) and purified by flash silica chromatography. The compounds were characterized by Bruker Avance III NMR spectrometer at room temperature at frequencies of 500 MHz (¹H), 126 MHz (¹³C), and 471 MHz (¹⁹F) in CDCl₃ or DMSO-d₆ as the solvents. Chemical shifts (δ) were recorded in ppm and coupling constants (*J*) in Hz. The molecular mass was determined by ESI and MALDI/TOF analyzer using α -cyano-4-hydroxycinnamic acid (HCCA) as the matrix. UV-visible-NIR spectra were recorded by an Aligent CARY5000 spectrometer (Agilent, USA). Fluorescence spectra were collected on a Perkin Elmer LS55 using a 1 cm path length quartz cell.

3.2 Research Design and Methodology

Synthesis of *N,N'*-((5,5-difluoro-3,7-bis(4-methoxyphenyl)-5*H*-4 λ^4 ,5 λ^4 -dipyrrolo[1,2-*c*:2',1'-*f*][1,3,5,2]triazaborinine-1,9-diyl)bis(3,1-phenylene))bis(1-((2*R*,3*R*,4*S*,5*S*,6*R*)-3,4,5-trihydroxy-6-(hydroxymethyl)tetrahydro-2*H*-pyran-2-yl)-1*H*-1,2,3-triazole-4-carboxamide) (AZB-Glc)

AZB-P (50.2 mg, 0.070 mmol) was dissolved in dimethyl sulfoxide (DMSO, 10.0 mL) and then 1-azido β -*D*-glucopyranose (44.4 mg, 0.213 mmol) was added to the solution. After stirring for 15 min at 25 °C, a solutions of freshly prepared sodium ascorbate (0.213 mmol, 0.5 M in water), followed by copper (II) sulfate pentahydrate (CuSO₄·5H₂O, 0.213 mmol, 0.5 M in water) were added into the mixture. The reaction was stirred vigorously at 25 °C for 12 h. After that, the mixture was extracted with ethyl acetate (20 mL), and the organic layer was removed under reduced pressure. Next, the residue was dissolved in methanol and precipitated in diethyl ether. The precipitate was filtered out and washed with diethyl ether and hexane to yield 48.2 mg (62.5 %) of AZB-Glc as a green solid. ¹H NMR (500 MHz, DMSO) δ 10.53 (s, 2H), 8.95 (s, 2H), 8.42 (s, 2H), 8.15 (d, *J* = 8.4 Hz, 4H), 7.96 (d, *J* = 7.5 Hz, 2H), 7.81 (d, *J* = 7.9 Hz, 2H), 7.46 (s, 3H), 7.45 – 7.34 (m, 2H), 7.12 (d, *J* = 8.5 Hz, 4H), 5.64 (d, *J* = 9.1 Hz, 2H), 5.48 (d, *J* = 5.7 Hz, 2H), 5.32 (d, *J* = 4.4 Hz, 2H), 5.19 (d, *J* = 5.1 Hz, 2H), 4.66 (d, *J* = 5.3 Hz, 2H), 3.86 (s, 6H), 3.68 (d, *J* = 4.3 Hz, 4H). ¹³C NMR (126 MHz, DMSO) δ 162.5, 158.7, 157.9, 144.9, 143.1, 142.8, 139.2, 132.5, 132.2, 129.4, 127.2, 125.6, 123.6, 122.3, 121.6, 120.3, 114.9, 88.3, 80.5, 77.2, 72.6, 69.9, 61.2, 56.0. HRESI-MS (*m/z*): calcd for C₅₂H₅₀BF₂N₁₁O₁₄Na [M+Na]⁺, 1124.3501 found 1124.3483

Synthesis of *N,N'*-((5,5-difluoro-2,8-diiodo-3,7-bis(4-methoxyphenyl)-5*H*-4 λ^4 ,5 λ^4 -dipyrrolo[1,2-*c*:2',1'-*f*][1,3,5,2]triazaborinine-1,9-diyl)bis(3,1-phenylene))dipropiolamide (AZB-PI)

Under N₂ atmosphere, AZB-P (53.0 mg, 0.077 mmol) and *N*-iodosuccinimide (NIS, 34.6 mg, 0.154 mmol) were mixed in chloroform/acetic acid (CHCl₃/CH₃COOH, 3:1, 4 mL), then the mixture was stirred overnight at 25 °C. Afterwards, the organic layer was separated and washed with sodium thiosulfate (Na₂S₂O₃, 2 × 50 mL), sodium

bicarbonate (NaHCO_3 , 2 × 50 mL) and brine (20 mL). The organic layer was dried over anhydrous sodium sulfate (anh. Na_2SO_4), and the solvent was removed under reduced pressure. The residue was purified by flash silica chromatography (silica gel, ethyl acetate/hexanes, 1/1, v/v) to yield 63.1 mg (87 %) of **AZB-PI** as a green solid. ^1H NMR (500 MHz, DMSO) δ 10.20 (s, 2H), 7.26 (s, 2H), 6.84 (d, J = 8.1 Hz, 2H), 6.78 (d, J = 8.6 Hz, 4H), 6.68 (d, J = 7.7 Hz, 2H), 6.60 (t, J = 7.9 Hz, 2H), 6.25 (d, J = 8.7 Hz, 4H), 3.67 (s, 2H), 3.02 (s, 6H). ^{13}C NMR (126 MHz, DMSO) δ 161.7, 160.9, 150.2, 147.3, 144.9, 138.5, 132.7, 128.9, 127.3, 123.3, 121.5, 120.9, 113.9, 86.7, 78.8, 77.9, 55.8. MALDI-TOF MS (m/z): calcd for $\text{C}_{40}\text{H}_{27}\text{BF}_2\text{N}_5\text{O}_4$ [$\text{M}+\text{H}$] $^+$: 944.303, found: 944.350, and $\text{C}_{40}\text{H}_{26}\text{BF}_2\text{N}_5\text{O}_4\text{Na}$ [$\text{M}+\text{Na}$] $^+$: 966.249, found: 966.731.

Synthesis of N,N' -((5,5-difluoro-2,8-diiodo-3,7-bis(4-methoxyphenyl)-5*H*-4 λ^4 ,5 λ^4 -dipyrrolo[1,2-*c*:2',1'-*f*][1,3,5,2]triazaborinine-1,9-diyl)bis(3,1-phenylene))bis(1-((2*R*,3*R*,4*S*,5*S*,6*R*)-3,4,5-trihydroxy-6-(hydroxymethyl)tetrahydro-2*H*-pyran-2-yl)-1*H*-1,2,3-triazole-4-carboxamide)(AZB-Glc-I)

AZB-PI (33.2 mg, 0.034 mmol) was dissolved in a mixture of chloroform, ethanol, and water (CHCl_3 , EtOH and water, 6:1:1, v/v, 8 mL). Then, 1-Azido β -D-glucopyranose (28.7 mg, 0.140 mmol), sodium ascorbate (4.90 mg, 0.0248 mmol), copper (II) sulfate pentahydrate ($\text{CuSO}_4 \cdot 5\text{H}_2\text{O}$, 3.50 mg, 0.014 mmol) were added into the mixture, and the mixture was stirred vigorously at 25 °C for 24 h. After that, the resulting mixture was extracted with ethyl acetate (20 mL), and the organic layer was removed under reduced pressure. Next, the residue was dissolved in methanol and precipitated in diethyl ether. The precipitate was filtered out and washed with diethyl ether and hexane to yield 9.0 mg (19 %) of **AZB-Glc-I** as a green solid. ^1H NMR (500 MHz, DMSO) δ 10.68 (s, 2H), 8.99 (s, 2H), 8.40 (s, 2H), 7.82 (d, J = 7.6 Hz, 2H), 7.62 (d, J = 8.1 Hz, 4H), 7.55 (d, J = 7.3 Hz, 1H), 7.42 – 7.34 (m, 2H), 7.08 (d, J = 8.3 Hz, 4H), 5.66 (d, J = 9.0 Hz, 2H), 5.48 (d, J = 5.4 Hz, 2H), 5.31 (d, J = 4.2 Hz, 2H), 5.18 (d, J = 5.0 Hz, 2H), 4.64 (s, 2H), 3.85 (s, 6H), 3.71 (d, J = 8.5 Hz, 4H). ^{13}C NMR (126 MHz, DMSO) δ 161.2, 160.4, 158.4, 147.2, 144.5, 142.7, 138.4, 132.6, 132.3, 132.0, 128.3, 127.4, 126.8, 123.0, 113.9, 113.49, 113.0, 87.9, 80.1, 76.7, 72.2, 69.4, 60.8, 55.4. ^{19}F NMR (471 MHz, DMSO) δ -130.48 (q,

BF₃). HRESI-MS (m/z): calcd for C₅₂H₄₈BF₂I₂N₁₁O₁₄Na [M+Na]⁺: 1376.1434, found 1376.1437.

3.3 General Details for Vis-NIR and Fluorescence Measurements and Quantum Yield Calculations

The stock solutions of **AZB-Glc** and **AZB-Glc-I** were prepared by dissolving 1.5 mg of **AZB-Glc** and 1.2 mg of **AZB-Glc-I** in DMSO in a 3 mL standard volumetric flask to make the final concentrations of 4.5×10^{-4} M for **AZB-Glc** and 3.0×10^{-4} M for **AZB-Glc-I**.

3.3.1 Vis-NIR Absorption Measurement

The stock solutions of **AZB-Glc** and **AZB-Glc-I** (10 μ L) were added to 3.0 mL of solvents in 3.5 mL quartz cuvettes (final concentrations $\sim 1.5 \mu$ M for **AZB-Glc** and $\sim 1.0 \mu$ M for **AZB-Glc-I**). The Vis-NIR absorption spectra were recorded by a Cary Series UV-Vis-NIR spectrophotometer (Agilent Tech, Santa Clara, CA, USA).

3.3.2 Fluorescence Measurement

The stock solutions of **AZB-Glc** and **AZB-Glc-I** (10 μ L) were added to 3.0 mL of solvents in 3.5 mL quartz cuvettes (final concentrations $\sim 1.5 \mu$ M for **AZB-Glc** and $\sim 1.0 \mu$ M for **AZB-Glc-I**). The fluorescence spectra were recorded by a Perkin Elmer LS55 fluorescence spectrometer, using the following parameters: excitation wavelengths = 670 nm, excitation slit widths = 10 nm, and emission slit widths = 10 nm.

The fluorescence quantum yields (Φ_f) which define as the ratio of the number of photons emitted to the number of photons absorbed were calculated using equation (1) and relating to Zn-pthalocyanine in pyridine as a standard (std) ($\Phi_{std} = 0.30$).

$$\Phi_f = \Phi_{std} \times \left(\frac{A_{sample}}{A_{std}} \right) \times \left(\frac{I_{std}}{I_{sample}} \right) \times \left(\frac{\eta_{sample}}{\eta_{std}} \right)^2 \dots\dots (1)$$

where Φ denotes fluorescence quantum yield, A is the peak area of emission, I is the absorbance at the excitation wavelength, and η stands for the solvent reflective index.

3.4 Singlet-Oxygen Generation Measurements

A solution of ethanol containing 80 μM of 1,3-diphenylisobenzofuran (DPBF, singlet oxygen scavenger) and 0.5 μM of **AZB-Glc-I** in a quartz cell of 1 cm path length was exposed to a red LED lamp (660 nm, power density of 8.7 mW cm⁻²) at room temperature. Then, DPBF absorbance was measured at 408 nm in a microplate reader (BMG Labtech/SPECTROstar Nano) every 1-5 s intervals for 18 s. The DPBF solution in ethanol (negative control) and the solution containing 0.5 μM methylene blue (MB, comparative control) were also examined. The singlet oxygen quantum yield of **AZB-Glc-I** was determined by the reduction of DPBF absorbance over irradiation time. The singlet oxygen quantum yield was calculated according to equation (2).

$$\Phi_{\text{sample}} = \Phi_{\text{std}} \times \left(\frac{\text{grad}_{\text{sample}}}{\text{grad}_{\text{std}}} \right) \times \left(\frac{F_{\text{std}}}{F_{\text{sample}}} \right) \dots\dots (2)$$

where Φ_{std} denotes singlet oxygen quantum yield of methylene blue (0.52 in ethanol), grad is the rate of reaction, F is absorption correction factor ($F = 1 - 10^{-\text{absorbance}}$)

3.5 Cell Experiments

3.5.1 Cell Culture

Breast cancer (MCF-7 and MDA-MB-231) and human fetal lung fibroblast 1 (HFL1) cell lines were purchased from the American Type Culture Collection (ATCC). The cells were seeded in 75 cm² flasks containing culture media (Dulbecco's Modified Eagle Medium/High glucose, HyClone, for MCF-7 and MDA-MB-231; Kaighn's Modification of Ham's F-12 Medium, ATCC, for HFL1) supplemented with 10 % fetal bovine serum (FBS, Gibco) and 1 % penicillin-streptomycin (CORNING). All cells were incubated at 37 °C in a humidified atmosphere containing 5 % CO₂.

3.5.2 Cell imaging

Live Cell imaging: **AZB-Glc**, a non-iodinated Aza-BODIPY was chosen for imaging experiments due to its high fluorescence signal, which is useful for tumor detection. MCF-7, MDA-MB-231, and HFL1 cells were cultured on 8-well glass chamber slides (7×10^3 cells/well) in complete media for at least 24 h prior to treatment with **AZB-Glc** ($5 \mu\text{M}$). All treated cells were incubated for various time points (0, 1, 3, 6, and 24 h) at 37°C . After 3 times washing with PBS (pH 7.4), the cell nuclei were stained with Hoechst 33342 ($1.0 \mu\text{M}$). Then, live cells imaging was achieved with a Laser Scanning Confocal Microscope with a 60X oil immersion objective lens (LSCM, Nikon A1Rsi). Moreover, all the cells were treated with **AZB-P** at the same conditions to ensure the GLUT selectivity of **AZB-Glc**.

3.5.3 Co-Localization Analysis

MCF-7 and MDA-MB-231 cells were cultured on 8-well glass chamber slides for 24 h and then incubated with $5 \mu\text{M}$ of **AZB-Glc** for 6 h. After washing 3 times with PBS (pH 7.4), the cells were stained with LysoTracker™ Green DND-26 for 20 min. After that, the media were replaced with Hoechst 33342 containing DMEM. The cells were visualized by LSCM with a 60X oil immersion objective lens (Nikon A1Rsi).

3.5.4 D/L-Glucose Competition Test

MDA-MB-231 and MCF-7 cell lines were cultured on 8-well glass chamber slides in glucose-free complete DMEM media (7×10^3 cells/well) for 12 h. Thereafter, the cells were treated with glucose-free DMEM media containing various concentrations of *D*-glucose or *L*-glucose (0, 50, 100, and 200 mM) and **AZB-Glc** or **AZB-P** ($5 \mu\text{M}$) for 30 min before washing with PBS (pH 7.4). Cell nuclei were stained with Hoechst 33342 solution ($1.0 \mu\text{M}$) before visualizing under a LSCM with 60 X oil immersion objective lens (Nikon A1Rsi).

3.5.5 Combretastatin Treatment

The method was performed according to the protocol reported previously.¹⁷ In brief, MDA-MB-231 and MCF7 cultured on 8-well glass chamber slides (7×10^3

cells/well) were incubated with various concentrations of combretastatin (0, 0.1, and 1.0 μM) for 24 h in complete DMEM media. After media removal, the cells were incubated with **AZB-Glc** (5 μM) for 3 h. Then, the cells were washed with PBS buffer (pH 7.4) 3 times before staining the cell nucleus with Hoechst 33342. Fluorescence images of the cells were obtained under LSCM with a 60 X oil immersion objective lens (Nikon A1Rsi).

3.5.6 Light-Induced Cytotoxicity

The standard methyl thiazolyltetrazolium (MTT) assay was utilized to assess the PDT effect of the di-iodinated Aza-BODIPY analog (**AZB-Glc-I**) in three cell lines (MDA-MB-231, MCF7, and HF1 cells). The cells were cultured on 96-well plates in DMEM media for at least 24 h before treatment with various concentrations of **AZB-Glc-I** (0.125, 0.25, 1, 2.5, and 5 μM) for 6 h. After incubation, the cells were washed with PBS buffer (pH 7.4) 3 times, and fresh media were added before the cells were exposed to a red LED lamp (660 nm, power density of 8.7 mW cm^{-2}) at room temperature for 1 and 5 min. The control group was kept in the dark. Thereafter, all cells were incubated for another 24 h before treating with fresh PBS containing methyl thiazolyl tetrazolium (MTT reagent, 0.5 mg mL^{-1} , Sigma-Aldrich) for 2-3 h. Then, the media was replaced by DMSO to dissolve the resulting formazan. Relative cell viability was recorded by using a microplate reader (BMG Lab-tech / SPECTROstar Nano) to detect formazan adsorption at 560 nm.

3.5.7 Live/Dead Staining Assay

MDA-MB-231 cells were cultured on a 6-well plate (2×10^5 cells/well) in complete DMEM media for at least 24 h before incubating with **AZB-Glc-I** (2.5 μM) at 37 °C under 5% CO_2 for 6 h. After washing 3 times with PBS (pH 7.4), all cells were irradiated with a red LED lamp (660 nm, power density of 8.7 mW cm^{-2}) for 10 min at room temperature, and then re-incubated for another 24 h. After that, the cells were stained with 4 μM calcein acetoxymethyl (calcein-AM) and propidium iodide (PI) for 5 min and then wash with PBS (pH 7.4) before being visualized under a fluorescence microscope (BioRad/Zoe).

3.5.8 Intracellular Reactive Oxygen Detection

2,7-Dichloro-dihydro-fluorescein diacetate (DCFH-DA) was utilized to detect singlet oxygen in cell lines. MDA-MB-231 were seeded on 8-well glass chamber slides (7×10^3 cells/well) in complete DMEM media and cultured for at least 24 h before being incubated with **AZB-Glc-I** ($0.25 \mu\text{M}$) at 37°C under 5% CO_2 for 6 h. After washing 3 times with PBS (pH 7.4), the cells were treated with 2,7-dichloro-dihydro-fluorescein diacetate (DCFH-DA, $20 \mu\text{M}$, Sigma-Aldrich) for 1 h. Thereafter, the cells were washed with PBS (pH 7.4), the media replaced by fresh media, and the cells irradiated by the red LED lamp (660 nm, power density of 8.7 mW cm^{-2}) for 5 min. The control group was kept in the dark. All cells were stained with Hoechst 33342 before being visualized under LSCM with a 60X oil immersion objective lens (Nikon A1Rsi).

3.6 Statistical Analysis

One-way ANOVA followed by Tukey's post-hoc analysis was used for comparison between multiple groups using R studio. P values of less than 0.05 are considered significant (* $P < 0.05$, ** $P < 0.01$, *** $P < 0.001$). Pearson's correlation coefficient was calculated with the JACoP ImageJ plugin for the cell study. The half-maximal inhibitory concentration (IC_{50}) was determined by nonlinear regression analysis in GraphPad Prism 9.

CHAPTER IV

RESEARCH RESULTS

4.1 Results and Discussion

4.1.1 Synthesis and Photophysical Properties of AZB-Glc and AZB-Glc-I

terminal alkynes of an aza-BODIPY derivative (**AZB-P**) were generated via amide coupling between amino aza-BODIPY (**AZB-NH₂**) and propionic acids. **AZB-Glc** was synthesized through the azide-alkyne Huisgen cycloaddition, utilizing two azido-glucose moieties and **AZB-P**. In addition, the iodinated **AZB-PI** was employed instead of **AZB-P** in the synthesis of **AZB-Glc-I** (Figure 16 and Appendix A).

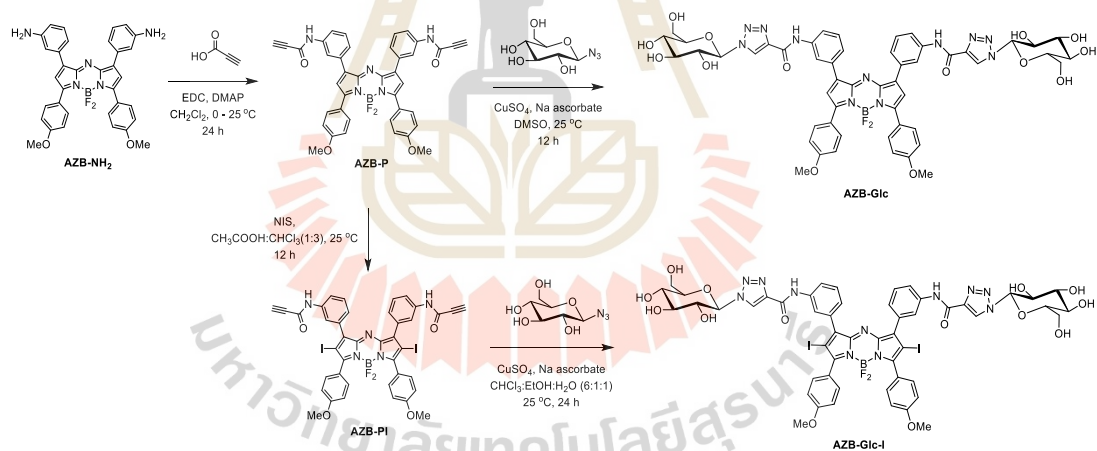


Figure 16 Synthesis of **AZB-Glc** and **AZB-Glc-I**.

4.1.2 Optical Properties of AZB-Glc and AZB-Glc-I

The photophysical characteristics of the glucose tracers (**AZB-Glc** and **AZB-Glc-I**) in different solvents were examined using VIS-NIR and fluorescence spectroscopy, as shown in Table 4 and Figure 17. The absorbance spectra revealed that the absorption maxima of both glucose tracers ranged from 675 to 705 nm in the NIR region, depending on the polarity and proticity of the solvents. Furthermore, in the case of **AZB-Glc**, the emission maxima in different solvents ranged from 716 to 733 nm, with a relatively high fluorescence quantum yield of approximately 0.40 to 0.65 in polar protic solvents (Table 4). Due to the effect of heavy atoms, **AZB-Glc-I** did not emit fluorescence, implying that only **AZB-Glc** can offer fluorescence imaging for the cancer diagnosis (Kamkaew et al., 2013).

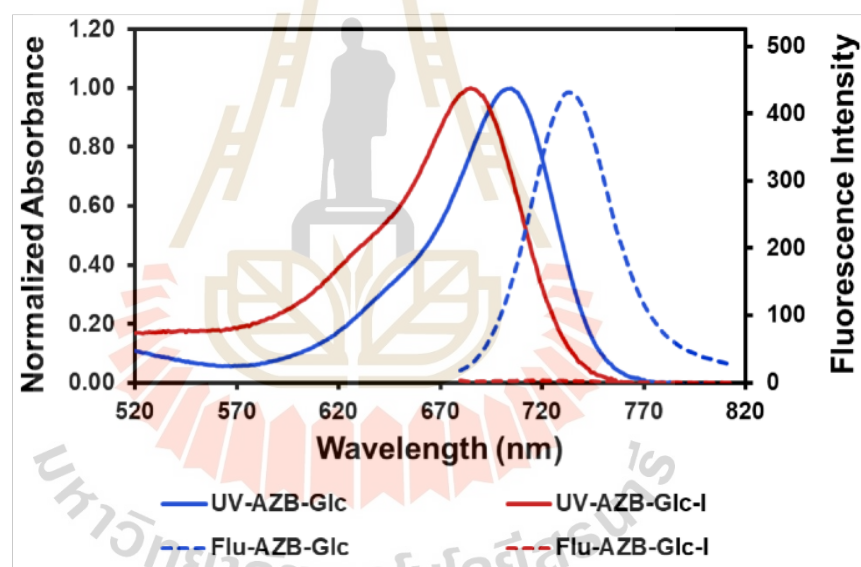


Figure 17 Absorption and fluorescence spectra of **AZB-Glc** (red line) and **AZB-Glc-I** (blue line) in DMSO.

Table 4 Photophysical properties of **AZB-Glc** and **AZB-Glc-I**.

Cpd	Solvent	λ_{\max} (nm)	ϵ^a ($M^{-1}cm^{-1}$) (n=3)	λ_{emiss}^b (nm)	$\Delta\lambda$ (nm)	Φ_f^c
AZB-Glc	CHCl ₃	705	1.5×10^4 ($\pm 0.03 \times 10^4$)	723	18	0.14
	DMSO	705	3.2×10^4 ($\pm 0.05 \times 10^4$)	733	28	0.40
	MeOH	688	0.9×10^4 ($\pm 0.06 \times 10^4$)	716	28	0.62
	PBS ^c	702	2.8×10^4 ($\pm 0.04 \times 10^4$)	726	24	0.45
AZB-Glc-I	CHCl ₃	687	2.8×10^4 ($\pm 0.05 \times 10^4$)		NF	
	DMSO	685	2.4×10^4 ($\pm 0.02 \times 10^4$)		NF	
	MeOH	675	0.5×10^4 ($\pm 0.04 \times 10^4$)		NF	
	PBS ^d	685	0.9×10^4 ($\pm 0.07 \times 10^4$)		NF	

^a the calculated average values of molar absorptivity from three distinct concentrations of **AZB-Glc** and **AZB-Glc-I**. ^b Samples [**AZB-Glc** (1.5 μM) and **AZB-Glc-I** (1.0 μM)] were excited at 670 nm. ^cRelative to Zn-phthalocyanine in pyridine ($\Phi_f = 0.30$). ^dPBS with 3% Tween-80. NF = No fluorescence.

4.1.3 Singlet Oxygen Generation Measurement *in Vitro* of **AZB-Glc-I**

The effectiveness of **AZB-Glc-I** in singlet oxygen generation was monitored by the absorption of 1,3-diphenylisobenzofuran (DPBF) as singlet oxygen (¹O₂) quencher. After exposing **AZB-Glc-I** to NIR light at 660 nm (power density of 8.7 mW cm⁻²), ¹O₂ was immediately produced as demonstrated by the reduction of DPBF absorbance at 408 nm (Figure 18 and 19), and the efficiency of ¹O₂ generation increased when increasing the exposure time. Besides, **AZB-Glc-I** could create ¹O₂ at a higher rate than methylene blue (standard photosensitizer) in an ethanol solution, which had a calculated ¹O₂ quantum yield (Φ_f) of 1.03 in comparison to methylene blue (Figure 20) implying that

the **AZB-Glc-I** could enhance the $^1\text{O}_2$ production, which suitable to be an excellent photosensitizer for cancer treatment by PDT.

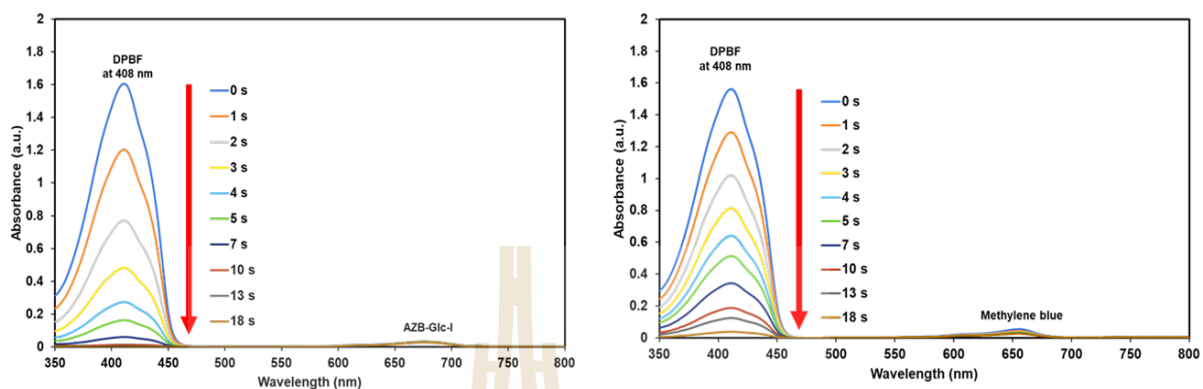


Figure 18 DPBF absorbance changes at 408 nm when being exposed to NIR light at various times in the presence of A) AZB-Glc-I, B) Methylene blue in ethanol.

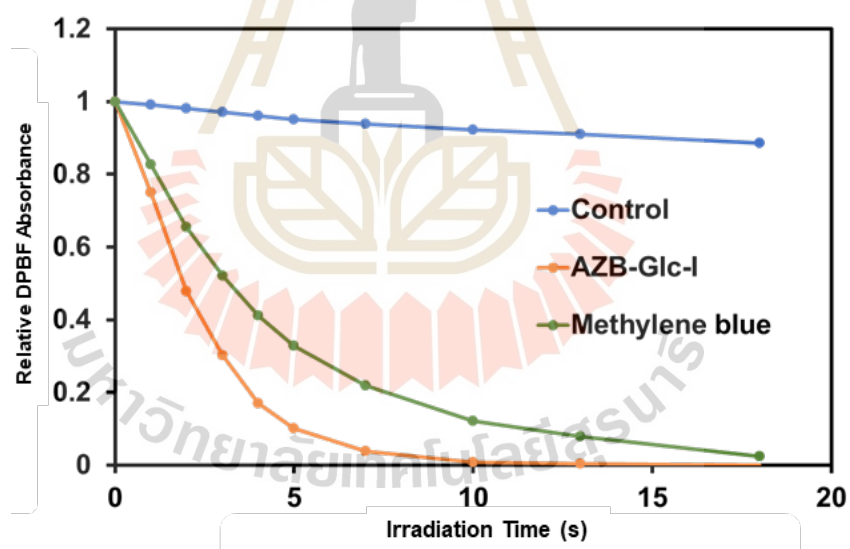


Figure 19 DPBF absorbance behavior in the presence of AZB-Glc-I ($0.5 \mu\text{M}$) and Methylene blue ($0.5 \mu\text{M}$) in ethanol under light irradiation for 18 s (1-5 s intervals).

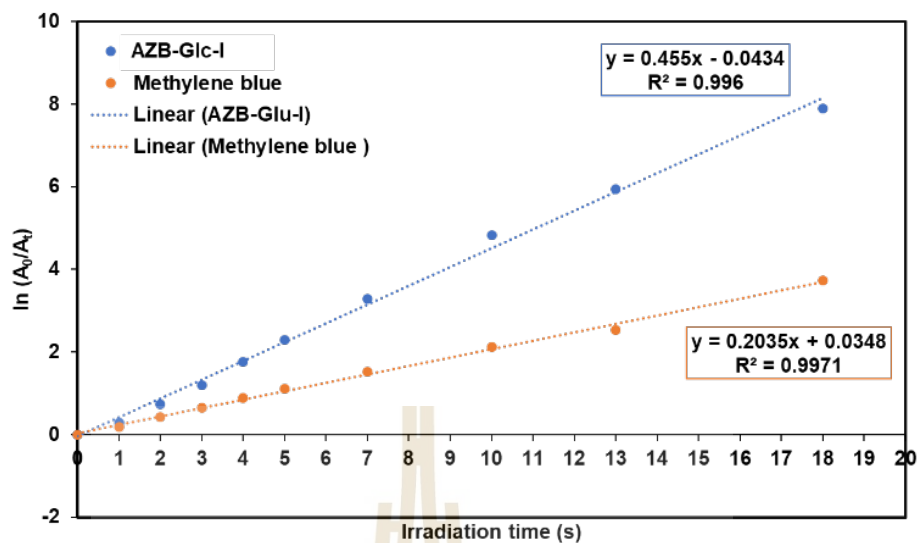


Figure 20 The first-order kinetic plot of DPBF absorbance at 408 nm vs irradiation times for calculating the $^1\text{O}_2$ quantum yield according to equation 2.

4.2 Cell Assays

4.2.1 Time-Dependent Cellular Uptake of AZB-Glc

As shown in table 4, **AZB-Glc** exhibited near-IR fluorescence with a high fluorescent quantum yield, whereas **AZB-Glc-I** exhibited almost no fluorescent emission. As a result, **AZB-Glc** was used as a fluorescent imaging probe to investigate the specific cellular uptake via GLUT. First, we visualized the cellular uptake of **AZB-Glc** between normal cells and cancer cells at different time points (0, 1, 3, 6 and 24 h) to evaluate the feasible application of the glucose tracer for molecular diagnostics and the optimal light irradiated time in PDT. High levels of GLUT1 cancer cells (MDA-MB-231 and MCF-7) (Barbosa and Martel, 2020; Hamann et al., 2018; Kang et al., 2002; Oh, Kim, Nam, and Shin, 2017) and a normal cell (HFL1) (Giatromanolaki et al., 2017; Ramu et al., 2018) were used for comparison. After 1 hour of incubation, **AZB-Glc** was accumulated in cancer cells, with fluorescent signals rising in a time-dependent manner (Figure 21). In contrast, almost no fluorescence was detected in the control cells during the same period (0-24 h). Notably, the Aza-BODIPY probe without glucose moieties (**AZB-P**) demonstrated fluorescent signals in cancer cells after 3 h of incubation, with no cancer cell selectivity (Figure 22). These findings possibly imply that the **AZB-Glc** binding GLUT response to cellular uptake. Higher levels of GLUTs

expression in cancer cells result in greater cellular uptake of the glucose tracers, allowing cancer cells to be distinguished from normal cells. Furthermore, **AZB-Glc** co-localized with LysoTracker in MDA-MB-231 and MCF-7 cells, with Pearson's coefficients of 0.78 and 0.85, respectively, demonstrating the build-up of the glucose tracer inside the lysosome in cancer cells and ensuring that the **AZB-Glc** inside the cancer cells (Figure 23).

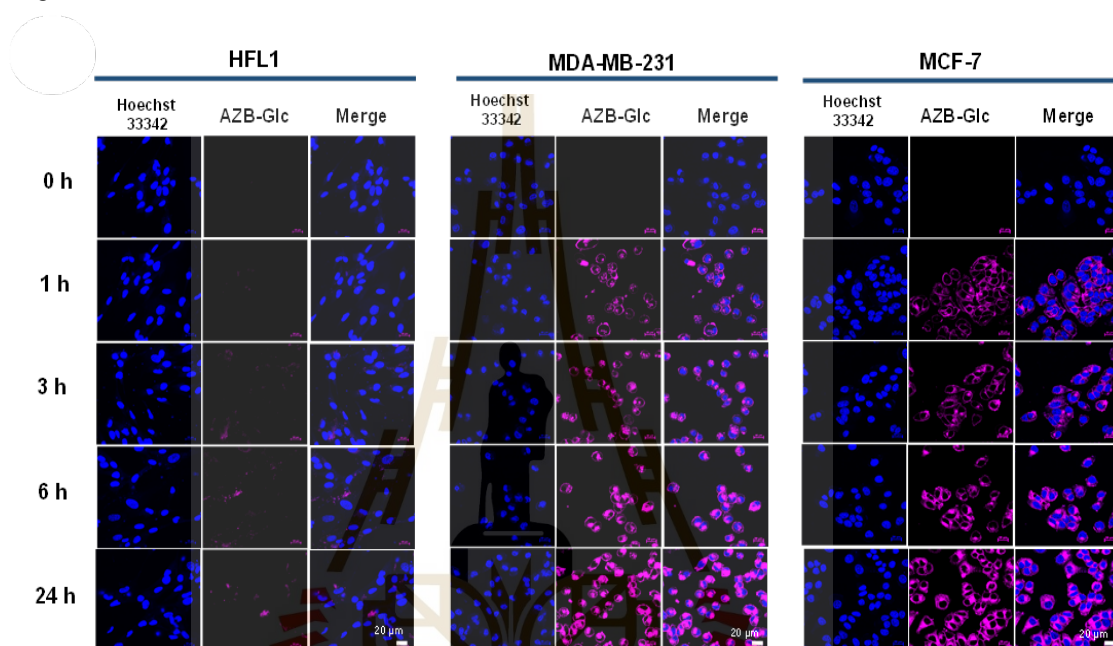


Figure 21 Time-Dependent Cellular Uptake of **AZB-Glc** ($5\mu\text{M}$) at different times of incubation (0,1,3,6 and 24h) in breast cancer cell lines (MAD-MB-231 and MCF-7) and human fetal lung fibroblasts (HFL1). Scale bar = $20\mu\text{m}$.

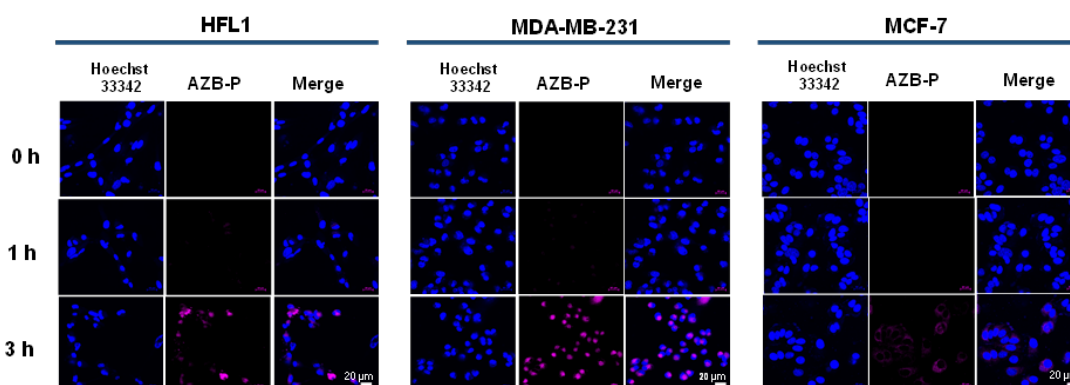


Figure 22 Time-Dependent Cellular Uptake of AZB-P ($5\mu\text{M}$) at different times of incubation (0,1 and 3 h) in breast cancer cell lines (MAD-MB-231 and MCF-7) and human fetal lung fibroblasts (HFL1). Scale bar = $20\mu\text{m}$.

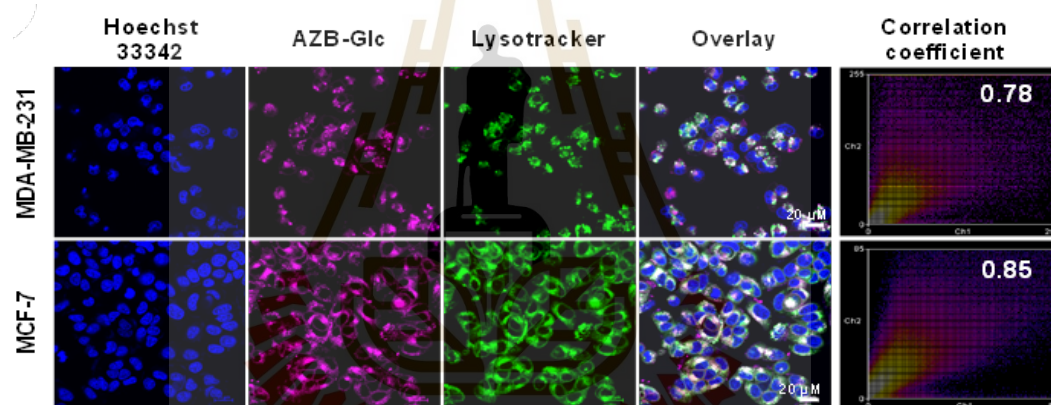


Figure 23 Co-localization experiment in the lysosome of AZB-Glc ($5\mu\text{M}$) in breast cancer cell lines (MAD-MB-231 and MCF-7) with Pearson's coefficients of 0.78 and 0.85, respectively. Scale bars = $20\mu\text{m}$.

4.2.2 D/L-Glucose Competition Assay of AZB-Glc

D/L-glucose competition assay was performed to validate the selectivity of AZB-Glc mediated GLUTs for cellular uptake in cancer cells. In glucose-free DMEM media, GLUTs-overexpressed MDA-MB-231 and MCF-7 cells were treated with AZB-Glc ($5\mu\text{M}$) in the presence of various doses of D- or L-glucose (0 to 200 mM) for 30 min before confocal imaging. As a result, increasing D-glucose concentration resulted in reduced red fluorescence signals in the cancer cell, but was not significantly different from L-glucose (Figure 4). In contrast, there was no difference in fluorescence signals when

AZB-P was used instead of AZB-Glc (Figure 24 and Figure 25), indicating that glucose moieties are important in cellular internalization.

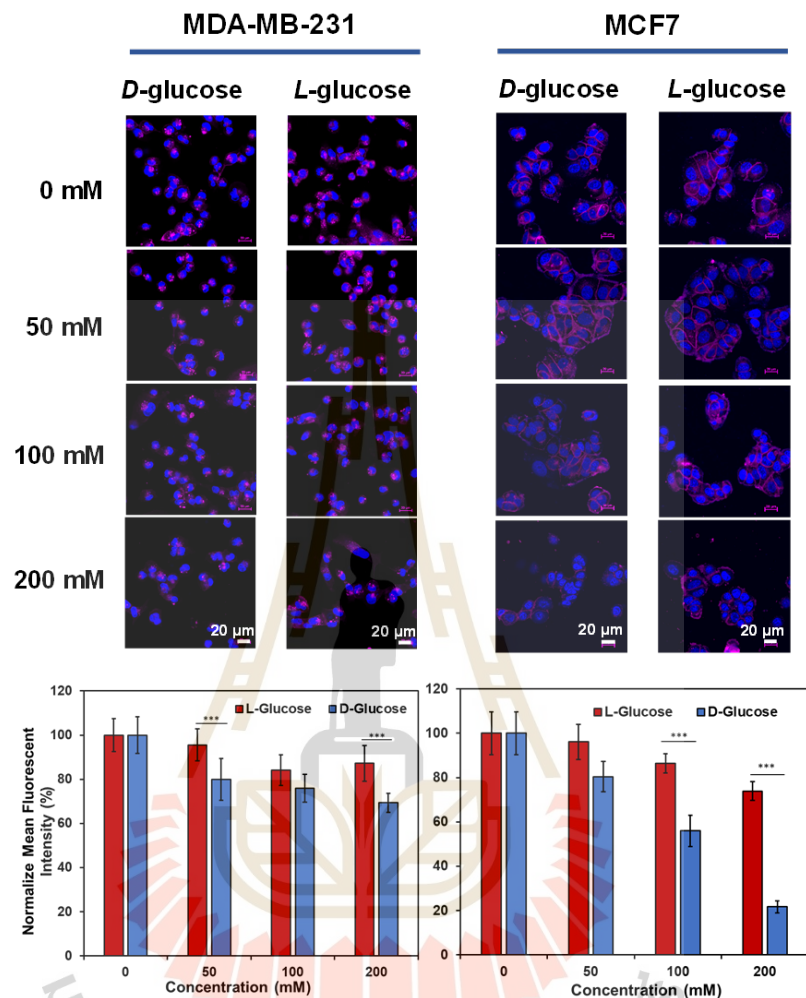


Figure 24 Glucose competition assay between AZB-Glc ($5 \mu\text{M}$) and various doses of *D-/L*-Glucose in MDA-MB-231 and MCF-7 cells (blue = nucleus, pink = AZB-Glc) and its quantitative analysis (data are presented as means \pm SD, $n = 40$). * $P < 0.05$, ** $P < 0.01$, and *** $P < 0.001$ using one-way ANOVA (Tukey test). Scale bars = $20 \mu\text{m}$.

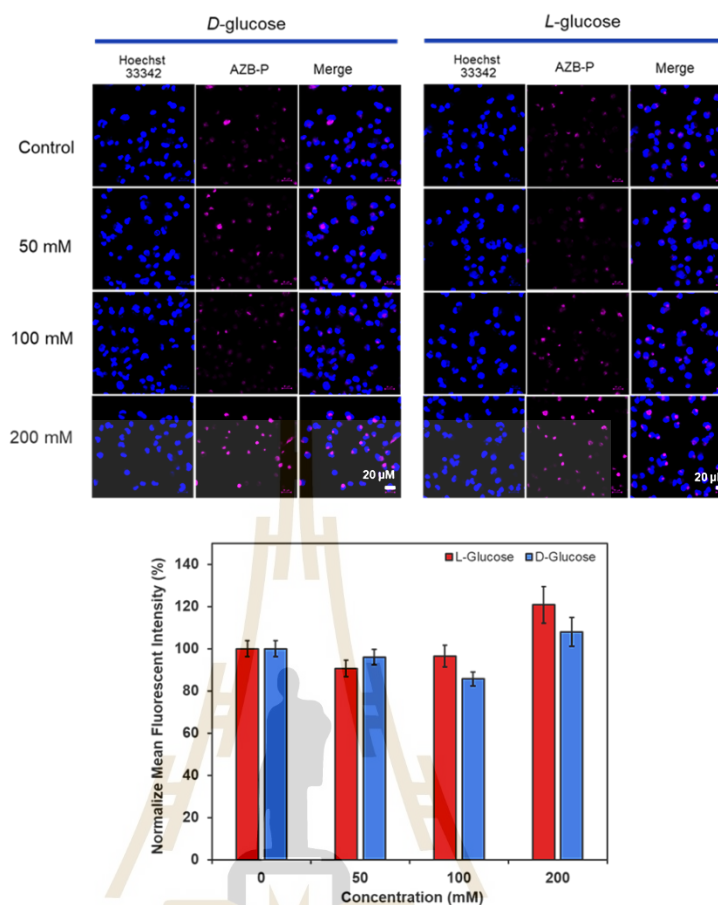


Figure 25 Glucose competition assay between AZB-P (5 μM) and various doses of D-/L-Glucose in MDA-MB-231 cells (blue = nucleus, pink = AZB-P) and its quantitative analysis (data are presented as means \pm SD, $n = 40$). * $P < 0.05$, ** $P < 0.01$, and *** $P < 0.001$ using one-way ANOVA (Tukey test). Scale bars = 20 μm .

4.2.3 Combretastatin Treatment

To further illustrate the biological applicability of AZB-Glc, the influence of anticancer drug treatment on glucose cellular uptake can be monitored by fluorescent image-based screening. As a model anticancer drug, we incubated the cancer cells with combretastatin, which has been associated with decreased cellular glucose uptake and cytoskeleton disruption (Karatoprak et al., 2020). In this experiment, Combretastatin (0.1 and 1.0 μM) was incubated in MDA-MB 231 and MCF-7 for 24 h. Then, washing with PBS and the cells were treated with AZB-Glc (5 μM) for 3 h. Cellular uptake of AZB-Glc was dramatically reduced in both cell lines, as shown in Figure 5.

This suggests that the probe can be used to monitor the suppression of tumor metabolism induced by anticancer therapy (Figure 26).

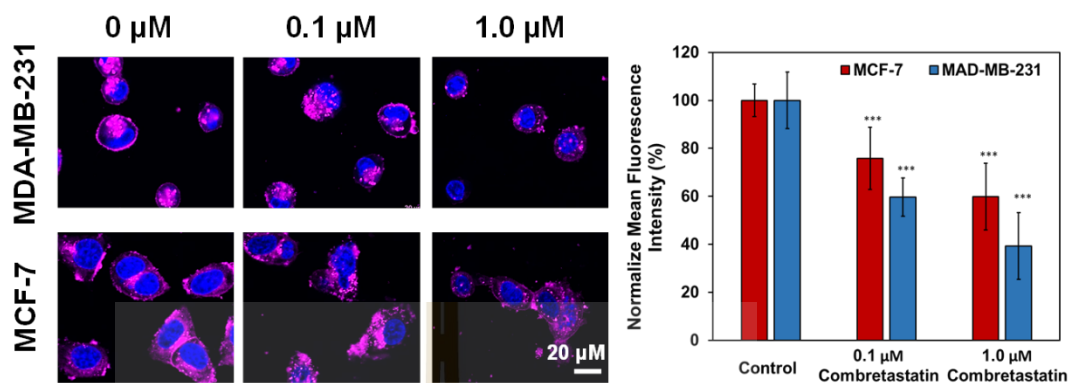


Figure 26 Confocal imaging of AZB-Glc in breast cancer cell (MCF-7 and MDA-MB-231) after being treated with Combretastatin (0.1 and 1 μM) for 3 h (blue = nucleus, pink = AZB-Glc) and its quantitative analysis (data are presented as means \pm SD (n = 30)). *P < 0.05, **P < 0.01, and ***P < 0.001 using one-way ANOVA (Tukey test). Scale bars = 20 μm .

4.2.4 Photocytotoxicity Assay of AZB-Glc-I

Based on all imaging experiments, it is evident that AZB-Glc can differentiate cancer cells from normal cells. To ensure the ability for cancer treatment by PDT, a series of photodynamic treatment studies was carried out using the iodinated form of aza-BODIPY (AZB-Glc-I) to generate $^1\text{O}_2$.

A photocytotoxicity assay of AZB-Glc-I was performed in both cancer cells (MDA-MB-231 and MCF-7) and normal cells (HFL1) to ensure the PDT efficacy of the probe using MTT assay. All cell lines were treated with various concentrations (0-5 μM) of AZB-Glc-I for 6 h before being exposed to NIR light (660 nm, power density of 8.7 mW cm^{-2}) for 1- and 5-min, and the cells were then allowed to proliferate for another 24 h in the dark. As shown in Figure 27A and B, cancer cells viability dramatically reduced in a dose-dependent manner even as irradiation time increased from 1 to 5 min. The half-maximum inhibitory concentration (IC_{50}) of AZB-Glc-I decreased approximately 7-fold when the exposure time was increased from 1 min to 5 min (Table 5). After 1 min of light exposure, the viability of normal cells was maintained at greater than 70% at

the highest measured concentration (5 μM) (Figure 27C). However, after a longer irradiation time, cell viability gradually drops as the dose of the probe increases, but the percentage of cell viability remains higher than that of cancer cells. Additionally, the IC_{50} values of **AZB-Glc-I** for HFL1 after 1 min of light exposure were approximately 20-fold greater than that of cancer cells, suggesting that the probes have the highest potential to become an effective therapeutic agent for cancer ablation under NIR light.

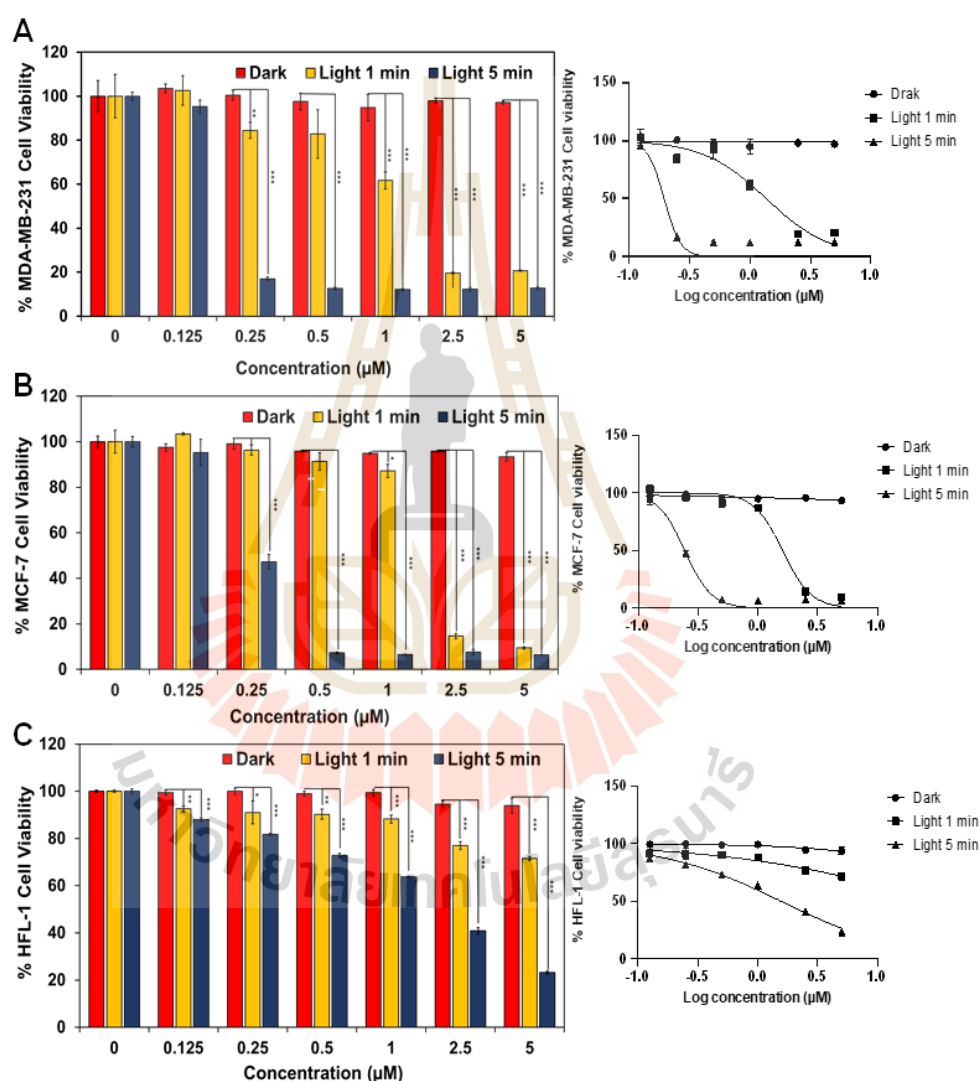


Figure 27 Photocytotoxicity experiment by MTT assay of the cells (MAD-MB-231, MCF-7, and HFL-1 cells) treated with various doses of **AZB-Glc-I** under NIR light at 660 nm (power density of 8.7 mW cm^{-2}) for 1 and 5 min of exposure times, and its half-maximal inhibitory concentration (IC_{50}) curves. (Data are presented as means \pm SD ($n = 3$). * $P < 0.05$, ** $P < 0.01$, and *** $P < 0.001$ using one-way ANOVA (Tukey test).

Table 5 The IC₅₀ values of **AZB-Glc-I** in different cell lines.

Cell line	IC ₅₀ (μ M)		
	dark	1 min	5 min
MDA-MB-231	>100	1.37***	0.20***
MCF-7	>100	1.61***	0.25***
HFL1	>100	31.95	1.57

*P < 0.05, **P < 0.01, and ***P < 0.001

4.2.5 Intracellular ¹O₂ Detection in MDA-MB-231 Created by AZB-Glc-I

In addition, to ensure the intracellular ¹O₂ generated by our probes, 2',7'-dichlorofluorescein diacetate (DCFH-DA) was used in this experiment because this dye (non-fluorescent) can be oxidized by ¹O₂ to form the 2',7'-dichlorofluorescein (DCF), which emit the green fluorescence. As can be seen in Figure 28, only MDA-MB-231 cells treated with **AZB-Glc-I** under light irradiation showed intense green fluorescence, indicating that ¹O₂ was created inside the cells. The green signals were undetectable in the control cell, the cell containing the probes in the dark, and the cells only exposed to light. This result confirmed that the NIR light-activated **AZB-Glc-I** generated ¹O₂ in the cellular environments.

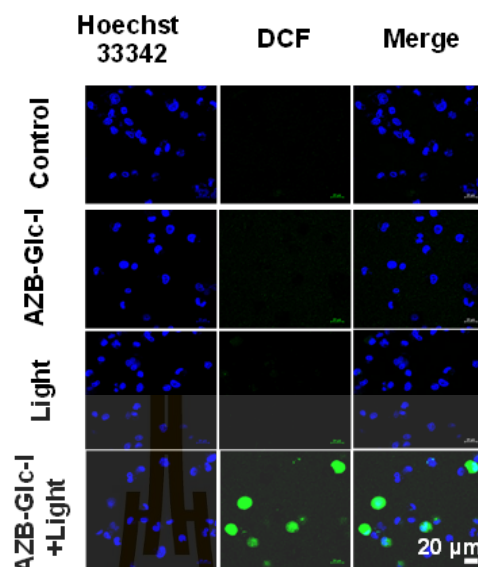


Figure 28 Intracellular $^1\text{O}_2$ detection in MDA-MB-231 cells treated with **AZB-Glc-I** (5 μM) only, NIR light at 660 nm (power density of 8.7 mW cm^{-2}) only, and **AZB-Glc-I** combined with NIR light. Blue = nucleus, light green = DCF. Scale bars = 20 μm .

4.2.6 Live/Dead Viability/Cytotoxicity of AZB-Glc-I in Breast Cancer Cells

live/dead viability/cytotoxicity was performed to further confirm that the cancer cells were destroyed by light-activated **AZB-Glc-I** in the living system. TO VISUALIZE VIABLE AND DEAD CELLS, the MDA-MB-231 cells were stained with calcein-AM and propidium iodide (PI). Calcein AM can react with intracellular esterase in a live cell and then display green fluorescence, whereas PI can only pass through the damaged cell membrane and emit red fluorescence by intercalation in the DNA of dead cells. After the cells were exposed to NIR light, red fluorescence of PI was evident in cells presenting **AZB-Glc-I**, showing that the light-activated **AZB-Glc-I** promotes cell death. On the other hand, the control cells, cells treated with **AZB-Glc-I** (no light irradiation), and cells irradiated without the probe mainly remained alive, as seen by the bright green fluorescence of calcein AM (Figure 29). This result consists of the previously reported photocytotoxicity in the MTT assay, which ensures that the **AZB-Glc-I** can be triggered by NIR light to damage the cell and showed no toxicity in the dark. Therefore, **AZB-Glc-I** could be a suitable therapeutic agent in cancer ablation.

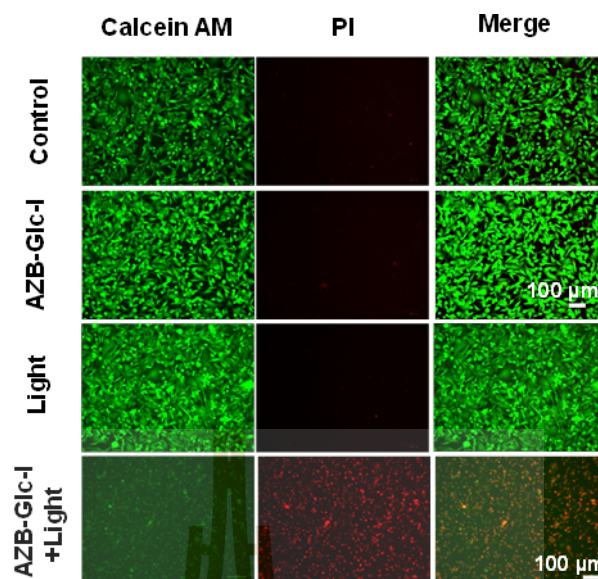


Figure 29 Live/dead cell viability/cytotoxicity assay in MDA-MB-231 cells treated with AZB-Glc-I ($5 \mu\text{M}$) only, NIR light at 660 nm (power density of 8.7 mW cm^{-2}) only, and AZB-Glc-I combined with NIR light. Green indicates the live cells from calcein AM, and red indicates the dead cells from PI. Scale bars = $20 \mu\text{m}$.

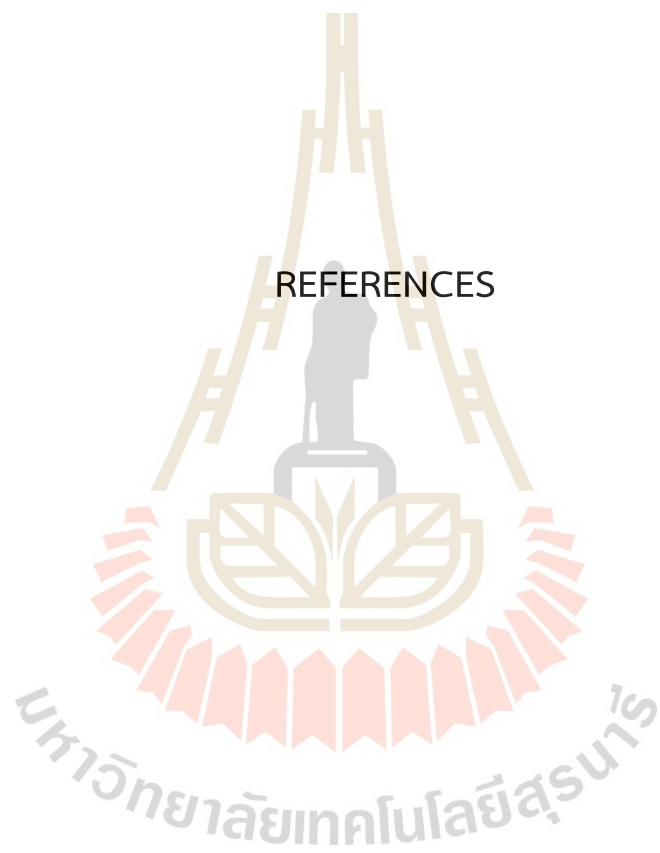


CHAPTER V

CONCLUSIONS

In conclusion, I succeeded in synthesizing the derivatives of aza-BODIPYs (**AZB-Glc** and **AZB-Glc-I**) as glucose tracers that target GLUT overexpression for cancer diagnosis and treatment via PDT. Both probes exhibited absorption wavelengths in the NIR region. Furthermore, **AZB-Glc** displays high fluorescence quantum yield, whereas no fluorescence emission was observed from **AZB-Glc-I**, due to the heavy atom effect. High cellular uptake of our glucose tracer was observed in cancer cells with high expression of GLUTs, especially in breast cancer cells. In the presence of *D*-glucose, the fluorescence signal of the probe was reduced, implying the internalization of our probe via GLUTs. Cancer cells uptake more of our probes than normal cells, resulting in enhanced PDT efficiency. **AZB-Glc-I** displayed strong photocytotoxicity towards cancer cells, with an IC_{50} range of 1.3-1.6 μ M after exposure to red light for only 1 min, and the IC_{50} reduced to the sub-micromolar range after 5 min irradiation. Because of the difference in cellular uptake between normal and cancer cells, facilitated by its linked glucose moieties and high singlet oxygen generation, **AZB-Glc-I** offers great promise for clinical development as a targeted PDT agent.

REFERENCES



REFERENCES

- Agostinis, P., Berg, K., Cengel, K. A., Foster, T. H., Girotti, A. W., Gollnick, S. O., Hahn, S. M., Hamblin, M. R., Juzeniene, A., Kessel, D., Korbelik, M., Moan, J., Mroz, P., Nowis, D., Piette, J., Wilson, B. C., and Golab, J. (2011). Photodynamic therapy of cancer: an update. *CA Cancer J Clin*, 61(4), 250-281.
- Allison, R. R., and Moghissi, K. (2013). Photodynamic Therapy (PDT): PDT Mechanisms. *Clin Endosc*, 46(1), 24-29.
- Ancey, P. B., Contat, C., and Meylan, E. (2018). Glucose transporters in cancer - from tumor cells to the tumor microenvironment. *Febs j*, 285(16), 2926-2943.
- Bacellar, I. O. L., Tsubone, T. M., Pavani, C., and Baptista, M. S. (2015). Photodynamic Efficiency: From Molecular Photochemistry to Cell Death. *Int J Mol Sci*, 16(9), 20523-20559.
- Barbosa, A. M., and Martel, F. (2020). Targeting Glucose Transporters for Breast Cancer Therapy: The Effect of Natural and Synthetic Compounds. *Cancers*, 12(1), 154.
- Cheng, Y., Shabir, G., Li, X., Fang, L., Xu, L., Zhang, H., and Li, E. (2020). Development of a deep-red fluorescent glucose-conjugated bioprobe for in vivo tumor targeting. *Chem Commun (Camb)*, 56(7), 1070-1073.
- Cheng, Z., Levi, J., Xiong, Z., Gheysens, O., Keren, S., Chen, X., and Gambhir, S. S. (2006). Near-Infrared Fluorescent Deoxyglucose Analogue for Tumor Optical Imaging in Cell Culture and Living Mice. *Bioconjug Chem*, 17(3), 662-669.
- Dąbrowski, J. M., Pucelik, B., Regiel-Futyra, A., Brindell, M., Mazuryk, O., Kyzioł, A., Stochel, G., Macyk, W., and Arnaut, L. G. (2016). Engineering of relevant photodynamic processes through structural modifications of metallotetrapyrrolic photosensitizers. *Coord Chem Rev*, 325, 67-101.
- De Simone, B. C., Mazzone, G., Pirillo, J., Russo, N., and Sicilia, E. (2017). Halogen atom effect on the photophysical properties of substituted aza-BODIPY derivatives. *Phys Chem Chem Phys*, 19(3), 2530-2536.

- Devic, S. (2016). Warburg Effect - a Consequence or the Cause of Carcinogenesis? *J Cancer*, 7(7), 817-822.
- Egorova, K. S., and Ananikov, V. P. (2017). Toxicity of Metal Compounds: Knowledge and Myths. *Organometallics*, 36(21), 4071-4090.
- Escobedo, J. O., Rusin, O., Lim, S., and Strongin, R. M. (2010). NIR dyes for bioimaging applications. *Curr Opin Chem Biol*, 14(1), 64-70.
- Fang, Y., Zhang, W., Zhu, M., Chen, S., Liu, X., Lu, W., and Zhang, X. (2017). Characterization of a near-infrared fluorescent DCPO-tagged glucose analogue for cancer cell imaging. *J Photochem Photobiol B*, 166, 264-271.
- Gambhir, S. S. (2002). Molecular imaging of cancer with positron emission tomography. *Nat Rev Cancer*, 2(9), 683-693.
- Gao, M., Yu, F., Lv, C., Choo, J., and Chen, L. (2017). Fluorescent chemical probes for accurate tumor diagnosis and targeting therapy. *Chem Soc Rev*, 46(8), 2237-2271.
- Ge, Y., and O'Shea, D. F. (2016). Azadipyrromethenes: from traditional dye chemistry to leading edge applications. *Chem Soc Rev*, 45(14), 3846-3864.
- Giatromanolaki, A., Liousia, M., Arelaki, S., Kalamida, D., Pouliliou, S., Mitrakas, A., Tsolou, A., Sivridis, E., and Koukourakis, M. (2017). Differential effect of hypoxia and acidity on lung cancer cell and fibroblast metabolism. *Biochem Cell Biol*, 95(3), 428-436.
- Gorantla, J. N., Pengthaisong, S., Choknud, S., Kaewpuang, T., Manyum, T., Promarak, V., and Ketudat Cairns, J. R. (2019). Gram scale production of 1-azido- β -d-glucose via enzyme catalysis for the synthesis of 1,2,3-triazole-glucosides. *RSC Advances*, 9(11), 6211-6220.
- Gorman, A., Killoran, J., O'Shea, C., Kenna, T., Gallagher, W. M., and O'Shea, D. F. (2004). In Vitro Demonstration of the Heavy-Atom Effect for Photodynamic Therapy. *J Am Chem Soc*, 126(34), 10619-10631.
- Hamann, I., Krysz, D., Glubrecht, D., Bouvet, V., Marshall, A., Vos, L., Mackey, J. R., Wuest, M., and Wuest, F. (2018). Expression and function of hexose transporters GLUT1, GLUT2, and GLUT5 in breast cancer-effects of hypoxia. *Faseb j*, 32(9), 5104-5118.

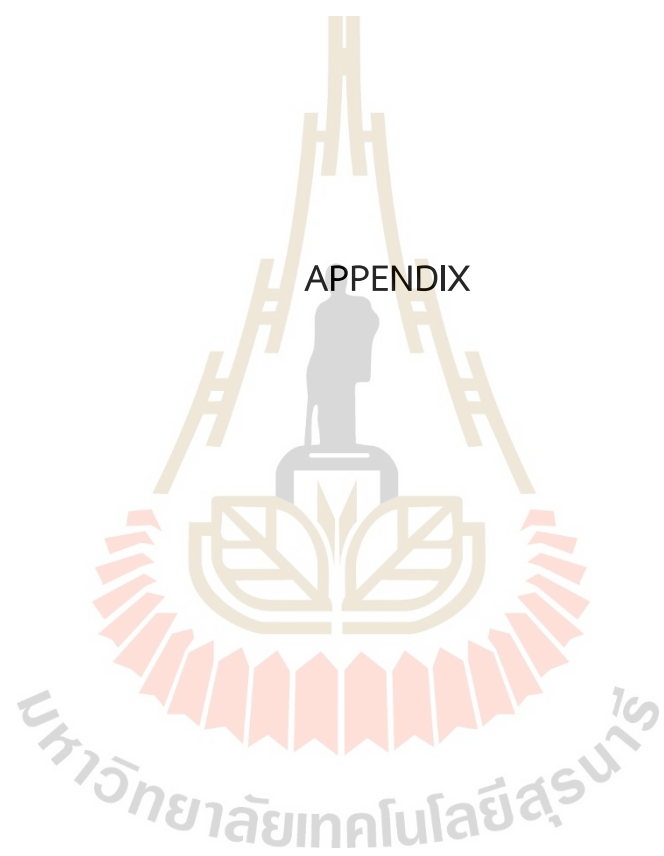
- Huang, Z. (2005). A review of progress in clinical photodynamic therapy. *Technol Cancer Res Treat*, 4(3), 283-293.
- Jo, A., Sung, J., Lee, S., Nam, H., Lee, H. W., Park, J., Kim, H. M., Kim, E., and Park, S. B. (2018). Near-IR Fluorescent Tracer for Glucose-Uptake Monitoring in Live Cells. *Bioconjug Chem*, 29(10), 3394-3401.
- Kamkaew, A., and Burgess, K. (2015). Aza-BODIPY dyes with enhanced hydrophilicity. *Chem Commun (Camb)*, 51(53), 10664-10667.
- Kamkaew, A., Lim, S. H., Lee, H. B., Kiew, L. V., Chung, L. Y., and Burgess, K. (2013). BODIPY dyes in photodynamic therapy. *Chem Soc Rev*, 42(1), 77-88.
- Kamkaew, A., Lim, S. H., Lee, H. B., Kiew, L. V., Chung, L. Y., and Burgess, K. (2013). BODIPY dyes in photodynamic therapy. *Chem Soc Rev*, 42(1), 77-88.
- Kang, S. S., Chun, Y. K., Hur, M. H., Lee, H. K., Kim, Y. J., Hong, S. R., Lee, J. H., Lee, S. G., and Park, Y. K. (2002). Clinical significance of glucose transporter 1 (GLUT1) expression in human breast carcinoma. *Jpn J Cancer Res*, 93(10), 1123-1128.
- Karatoprak, G. Ş., Küpeli Akkol, E., Genç, Y., Bardakci, H., Yücel, Ç., and Sobarzo-Sánchez, E. (2020). Combretastatins: An Overview of Structure, Probable Mechanisms of Action and Potential Applications. *Molecules*, 25(11), 2560.
- Koepsell, H. (2017). The Na(+)-D-glucose cotransporters SGLT1 and SGLT2 are targets for the treatment of diabetes and cancer. *Pharmacol Ther*, 170, 148-165.
- Kovar, J. L., Volcheck, W., Sevick-Muraca, E., Simpson, M. A., and Olive, D. M. (2009). Characterization and performance of a near-infrared 2-deoxyglucose optical imaging agent for mouse cancer models. *Anal Biochem*, 384(2), 254-262.
- Kubota, K. (2001). From tumor biology to clinical Pet: a review of positron emission tomography (PET) in oncology. *Ann Nucl Med*, 15(6), 471-486.
- Kue, C. S., Ng, S. Y., Voon, S. H., Kamkaew, A., Chung, L. Y., Kiew, L. V., and Lee, H. B. (2018). Recent strategies to improve boron dipyrromethene (BODIPY) for photodynamic cancer therapy: an updated review. *Photochem Photobiol Sci*, 17(11), 1691-1708.
- Laudanski, P., Swiatecka, J., Kovalchuk, O., and Wolczynski, S. (2003). Expression of GLUT1 gene in breast cancer cell lines MCF-7 and MDA-MB-231. *Ginekol Pol*, 74(9), 782-785.

- Lee, H. Y., Lee, J. J., Park, J., and Park, S. B. (2011). Development of fluorescent glucose bioprobes and their application on real-time and quantitative monitoring of glucose uptake in living cells. *Chemistry*, *17*(1), 143-150.
- Lin, H.-W., and Tseng, C.-H. (2014). A Review on the Relationship between SGLT2 Inhibitors and Cancer. *Int J Endocrinol*, *2014*, 719578-719578.
- Liu, X., Liu, S., Liu, X., Shi, Y., Yang, J., Huang, Z., Zhao, H., and Gao, Q. (2016). Fluorescent 6-amino-6-deoxyglycoconjugates for glucose transporter mediated bioimaging. *Biochem Biophys Res Commun*, *480*(3), 341-347.
- Macheda, M. L., Rogers, S., and Best, J. D. (2005). Molecular and cellular regulation of glucose transporter (GLUT) proteins in cancer. *J Cell Physiol*, *202*(3), 654-662.
- Maric, T., Mikhaylov, G., Khodakivskiy, P., Bazhin, A., Sinisi, R., Bonhoure, N., Yevtodiyenko, A., Jones, A., Muhunthan, V., Abdelhady, G., Shackelford, D., and Goun, E. (2019). Bioluminescent-based imaging and quantification of glucose uptake in vivo. *Nature Methods*, *16*(6), 526-532.
- Mueckler, M., and Thorens, B. (2013). The SLC2 (GLUT) family of membrane transporters. *Mol Asp Med*, *34*(2), 121-138.
- Ndagi, U., Mhlongo, N., and Soliman, M. E. (2017). Metal complexes in cancer therapy - an update from drug design perspective. *Drug Des Devel Ther*, *11*, 599-616.
- Oh, S., Kim, H., Nam, K., and Shin, I. (2017). Glut1 promotes cell proliferation, migration and invasion by regulating epidermal growth factor receptor and integrin signaling in triple-negative breast cancer cells. *BMB Rep*, *50*(3), 132-137.
- Park, J., Um, J. I., Jo, A., Lee, J., Jung, D.-W., Williams, D. R., and Park, S. B. (2014). Impact of molecular charge on GLUT-specific cellular uptake of glucose bioprobes and in vivo application of the glucose bioprobe, GB2-Cy3. *Chem Commun (Camb)*, *50*(66), 9251-9254.
- Pewklang, T., Chansaenpak, K., Lai, R. Y., Noisa, P., and Kamkaew, A. (2019). Aza-BODIPY probe for selective visualization of cyclooxygenase-2 in cancer cells. *Rsc Advances*, *9*(24), 13372-13377.
- Ramu, V., Gautam, S., Garai, A., Kondaiah, P., and Chakravarty, A. R. (2018). Glucose-Appended Platinum(II)-BODIPY Conjugates for Targeted Photodynamic Therapy in Red Light. *Inorg Chem*, *57*(4), 1717-1726.

- Rivenzon-Segal, D., Boldin-Adamsky, S., Seger, D., Seger, R., and Degani, H. (2003). Glycolysis and glucose transporter 1 as markers of response to hormonal therapy in breast cancer. *Int J Cancer*, 107(2), 177-182.
- Scheepers, A., Joost, H. G., and Schurmann, A. (2004). The glucose transporter families SGLT and GLUT: molecular basis of normal and aberrant function. *JPEN J Parenter Enteral Nutr*, 28(5), 364-371.
- Sola, R., and Bañuelos-Prieto, J. (2019). Introductory Chapter: BODIPY Dye, an All-in-One Molecular Scaffold for (Bio)Photonics. In.
- Speizer, L., Haugland, R., and Kutchai, H. (1985). Asymmetric transport of a fluorescent glucose analogue by human erythrocytes. *Biochim Biophys Acta*, 815(1), 75-84.
- Szablewski, L. (2013). Expression of glucose transporters in cancers. *Biochim Biophys Acta*, 1835(2), 164-169.
- Thomas, B., Yan, K.-C., Hu, X.-L., Donnier-Maréchal, M., Chen, G.-R., He, X.-P., and Vidal, S. (2020). Fluorescent glycoconjugates and their applications. *Chem Soc Rev*, 49(2), 593-641.
- van Straten, D., Mashayekhi, V., de Bruijn, H. S., Oliveira, S., and Robinson, D. J. (2017). Oncologic Photodynamic Therapy: Basic Principles, Current Clinical Status and Future Directions. *Cancers*, 9(2), 19.
- Vendrell, M., Samanta, A., Yun, S. W., and Chang, Y. T. (2011). Synthesis and characterization of a cell-permeable near-infrared fluorescent deoxyglucose analogue for cancer cell imaging. *Org Biomol Chem*, 9(13), 4760-4762.
- Warburg, O. (1956). On the origin of cancer cells. *Science*, 123(3191), 309-314.
- Wellberg, E. A., Johnson, S., Finlay-Schultz, J., Lewis, A. S., Terrell, K. L., Sartorius, C. A., Abel, E. D., Muller, W. J., and Anderson, S. M. (2016). The glucose transporter GLUT1 is required for ErbB2-induced mammary tumorigenesis. *Breast Cancer Res*, 18(1), 131.
- Yano, S., Hirohara, S., Obata, M., Hagiya, Y., Ogura, S.-i., Ikeda, A., Kataoka, H., Tanaka, M., and Joh, T. (2011). Current states and future views in photodynamic therapy. *J Photochem Photobiol C*, 12(1), 46-67.

- Yaylali, O., Kirac, F. S., and Yuksel, D. (2016). The role of 18F-FDG PET-CT in the detection of unknown primary malignancy: a retrospective study. *Turk J Med Sci*, 46(2), 474-482.
- Yeung, S. J., Pan, J., and Lee, M. H. (2008). Roles of p53, MYC and HIF-1 in regulating glycolysis - the seventh hallmark of cancer. *Cell Mol Life Sci*, 65(24), 3981-3999.
- Yoshioka, K., Takahashi, H., Homma, T., Saito, M., Oh, K. B., Nemoto, Y., and Matsuoka, H. (1996). A novel fluorescent derivative of glucose applicable to the assessment of glucose uptake activity of Escherichia coli. *Biochim Biophys Acta*, 1289(1), 5-9.
- Zambrano, A., Molt, M., Uribe, E., and Salas, M. (2019). Glut 1 in Cancer Cells and the Inhibitory Action of Resveratrol as A Potential Therapeutic Strategy. *Int J Mol Sci*, 20(13), 3374.
- Zhang, M., Zhang, Z., Blessington, D., Li, H., Busch, T. M., Madrak, V., Miles, J., Chance, B., Glickson, J. D., and Zheng, G. (2003). Pyropheophorbide 2-deoxyglucosamide: a new photosensitizer targeting glucose transporters. *Bioconjug Chem*, 14(4), 709-714.
- Zhang, X., Bloch, S., Akers, W., and Achilefu, S. (2012). Near-infrared molecular probes for in vivo imaging. *Curr Protoc Cytom*, Chapter 12, Unit12.27-Unit12.27.
- Zhao, M., Xu, Y., Xie, M., Zou, L., Wang, Z., Liu, S., and Zhao, Q. (2018). Halogenated Aza-BODIPY for Imaging-Guided Synergistic Photodynamic and Photothermal Tumor Therapy. *Adv Healthc Mater*, 7(18), 1800606.
- Zhou, Z., Song, J., Nie, L., and Chen, X. (2016). Reactive oxygen species generating systems meeting challenges of photodynamic cancer therapy. *Chem Soc Rev*, 45(23), 6597-6626.
- Zou, J., Yin, Z., Ding, K., Tang, Q., Li, J., Si, W., Shao, J., Zhang, Q., Huang, W., and Dong, X. (2017). BODIPY Derivatives for Photodynamic Therapy: Influence of Configuration versus Heavy Atom Effect. *ACS Appl Mater Interfaces*, 9(38), 32475-32481.

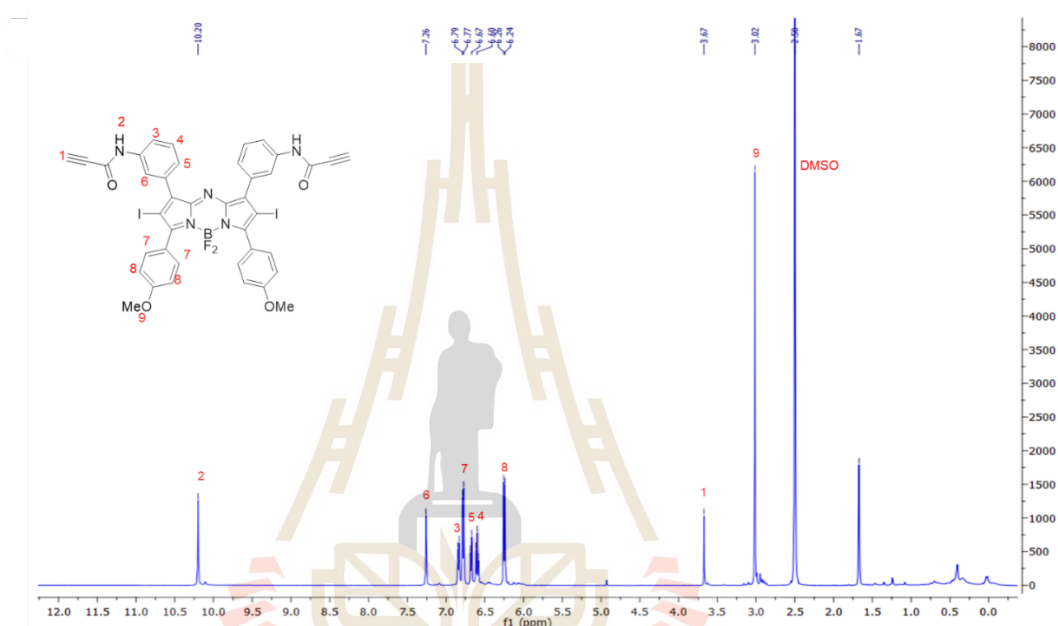
APPENDIX



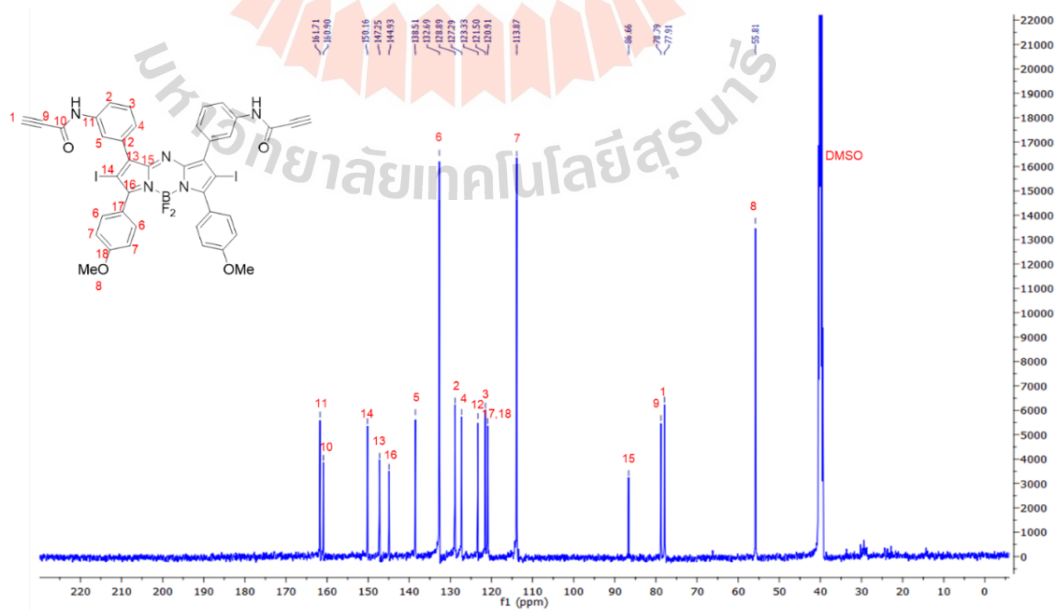
APPENDIX

SUPPORTING INFORMATION

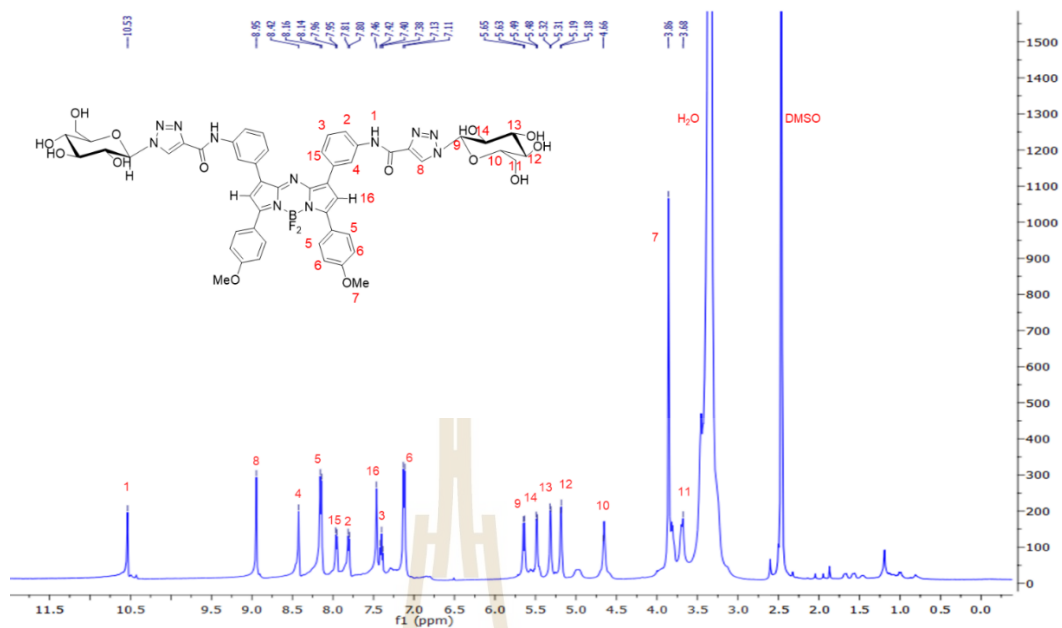
S1 ^1H and ^{13}C Nuclear Magnetic Resonance (NMR) Spectra



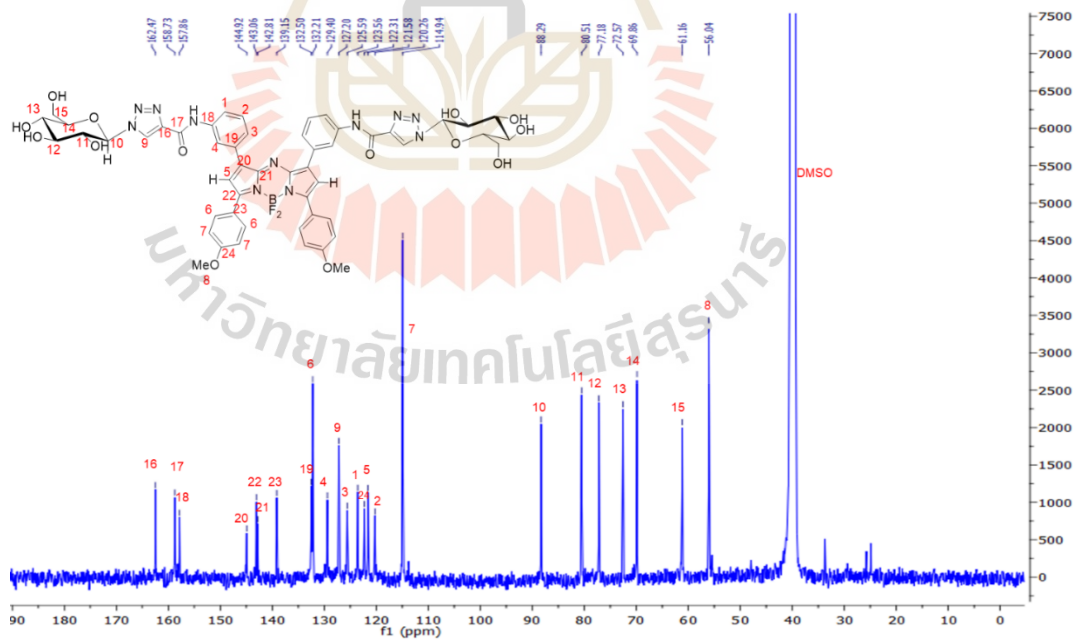
^1H NMR spectrum of AZB-PI.



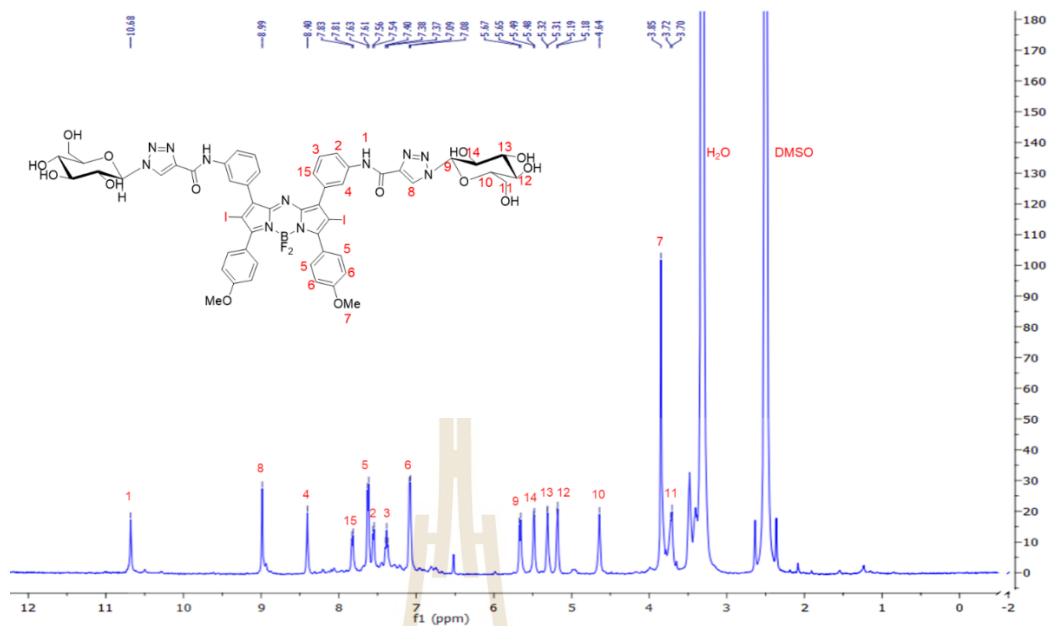
^{13}C NMR spectrum of AZB-PI.



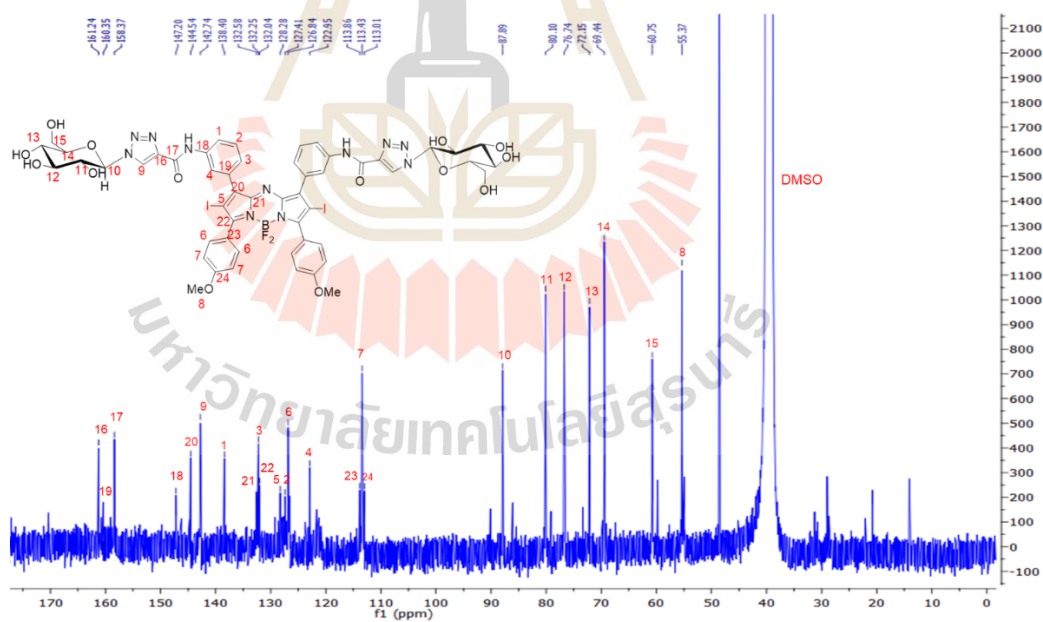
¹H NMR spectrum of AZB-Glc.



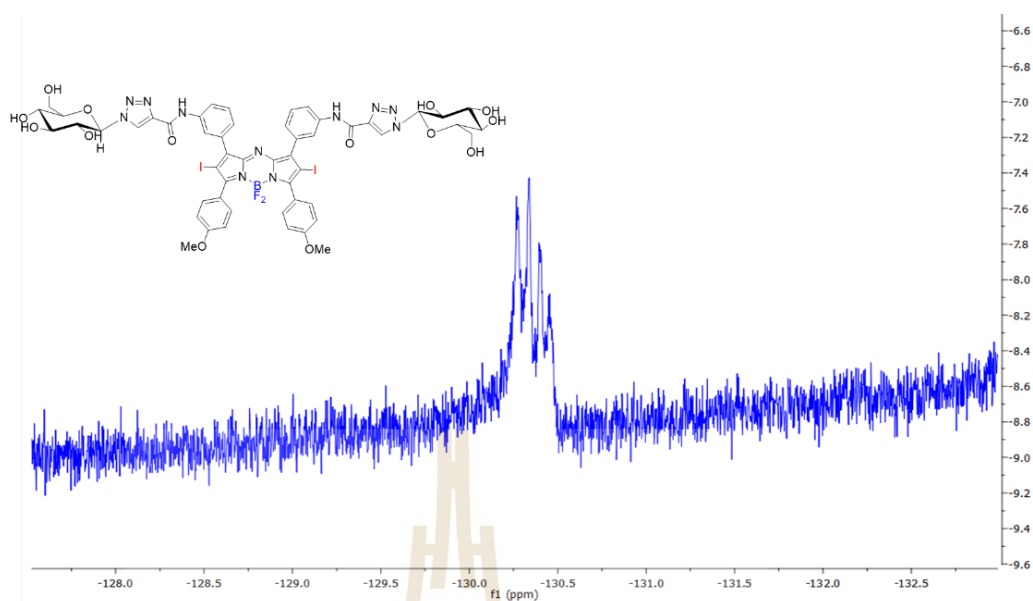
¹³C NMR spectrum of AZB-Glc.



¹H NMR spectrum of AZB-Glc-I.

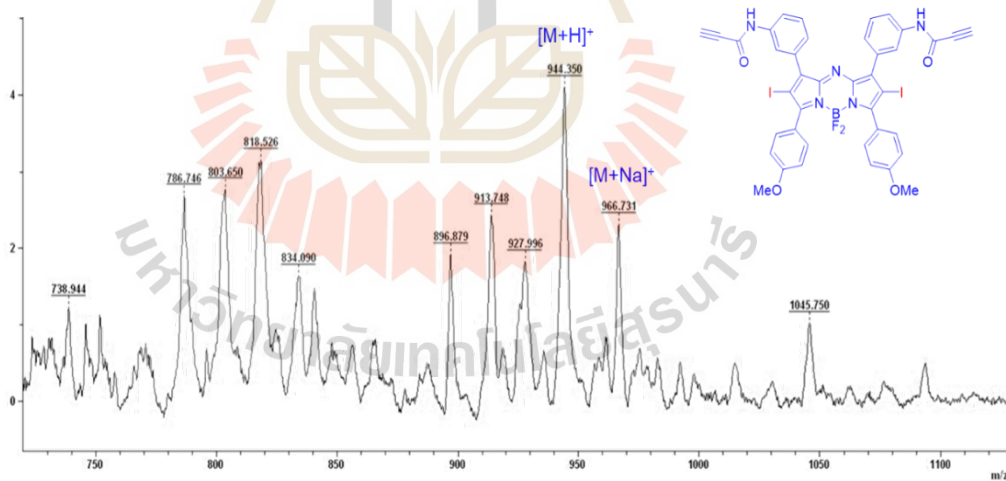


¹³C NMR spectrum of AZB-Glc-I.

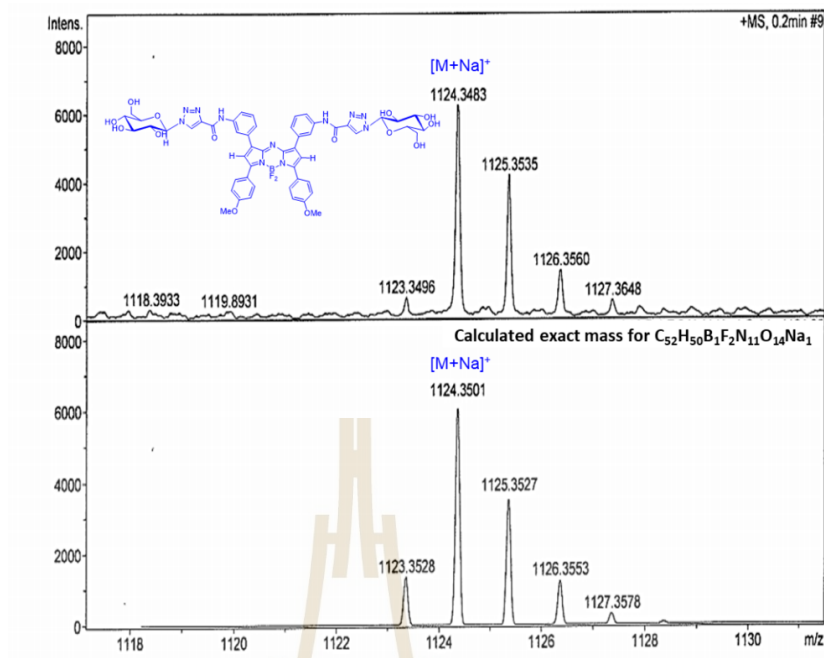


^{19}F NMR spectrum of AZB-Glc-I.

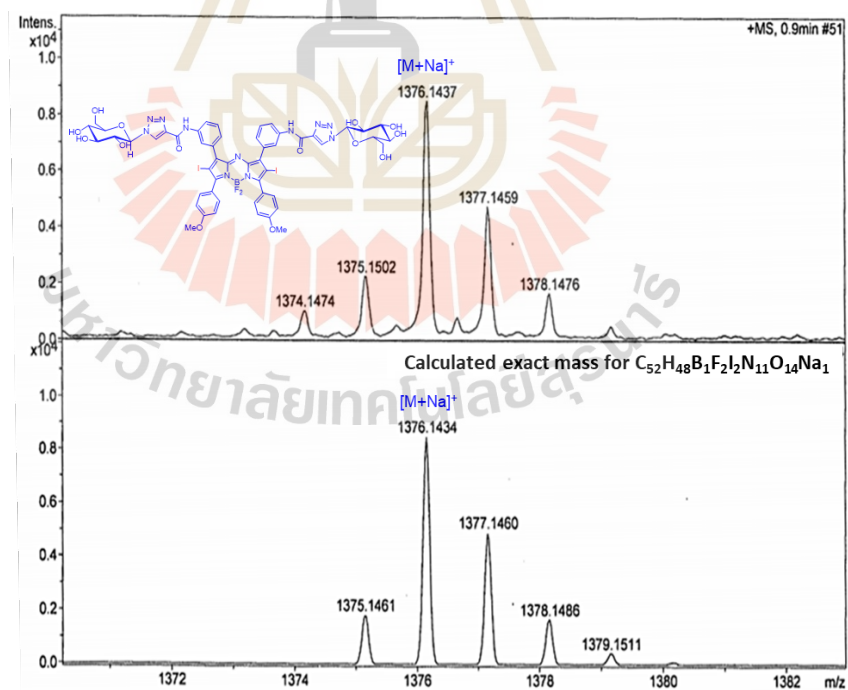
S2 Mass Spectrometry Results



Mass spectrum of AZB-PI.



Mass spectrum of AZB-Glc.



Mass spectrum of AZB-Glc-I.

CURRICULUM VITAE

Name: Jongjit Treekoon. **Phone number:** (+66)645146447

Address: 485/10 Payaptis Rd, Tambon Nai Mueang, Mueang Nakhon Ratchasima District, Nakhon Ratchasima 3000, Thailand **Email:** yuiyongyuy@gmail.com

Educational Background

- 2015-2019: *Bachelor's degree* :B.Sc) .Chemistry(, First class honors Suranaree University of Technology, Thailand.
- 2019-present: *Master's degree*: M.Sc. (Chemistry), dual degree program between Suranaree University of Technology, Thailand, and National Cheng Kung University, Taiwan under the supervision of Prof. Chen-Sheng Yeh and Asst. Prof. Anyanee Kamkaew.

Research Experience

- 2018: Responsive material and nanosensor laboratory, National Nanotechnology Center, Thailand -Working as a trainee under the supervision of Dr. Kantapat Chansaenpak and Asst. Prof. Anyanee Kamkaew.
- 2020-2021: Working and studying under a master's dual degree program with professional researchers at NCKU (Taiwan)

Research Publications

- **Treekoon, J.**, Chansaenpak, K., Tumcharern, G., Zaiman Zain, Z. S., Lee, H. B., Kue, C. S., and Kamkaew, A. (2021). Aza-BODIPY encapsulated polymeric nanoparticles as an effective nanodelivery system for photodynamic cancer treatment. *Materials Chemistry Frontiers*, 5(5), 2283-2293.
- **Treekoon, J.**, Pewklang, T., Chansaenpak, K., Gorantla, J. N., Pengthaisong, S., Lai, R.-Y., Ketudat-Cairns, J. R., and Kamkaew, A. (2021). Glucose conjugated aza-BODIPY for enhanced photodynamic cancer therapy. *Organic and Biomolecular Chemistry*, 19(26), 5867-5875.